WESTFÄLISCHE
WILHELMS-UNIVERSITÄT
MÜNSTER

MONTE CARLO GENERATORS FOR $t\bar{t}$ PRODUCTION

BACHELOR'S THESIS

Submitted by:
LUCA PAOLO WIGGERING

Westfälische Wilhelms-Universität Münster

Institut für Theoretische Physik

AG Klasen

First assessor: Prof. Dr. Michael Klasen

Second assessor: Priv.-Doz. Dr. Karol Kovařík

Münster, September 24, 2019

Declaration of Academic Integrity

I hereby confirm that this thesis is solely my own work and that I have used no sources or aids other than the ones stated. All passages in my thesis for which other sources, including electronic media, have been used, be it direct quotes or content references, have been acknowledged as such and the sources cited. All programs on the CD have been programmed by myself.

_____
(date and signature of student)

I agree to have my thesis checked in order to rule out potential similarities with other works and to have my thesis stored in a database for this purpose.

Münster, 11. September 2019

_____
(date and signature of student)

Contents

5   Conclusion and outlook   **43**

Bibliography   **45**

1 Introduction

The top quark is the heaviest of all known elementary particles with a mass similar to the one of a gold atom. Like the masses of the other elementary particles, the top mass is also a fundamental parameter of the Standard Model. In addition, the top mass is directly related to the cross section for the production of Higgs bosons [3, p. 1]. For this reason, the investigation of the top quark is not only essential for testing and measuring the Standard Model but also for exploring the Higgs sector.

The top quark was first discovered and measured at Tevatron, a proton-antiproton collider at Fermilab. After the Tevatron ceased operations in 2011, the top quark was further studied at the far more powerful Large Hadron Collider (LHC), a proton-proton collider at CERN. A large goal of the LHC is to find deviations from the Standard Model, so-called "new physics". To make this possible, precision calculations performed by theoretical physicists are necessary. Therefore, the subject of this work aims at verifying leading order predictions for the top quark pair-production cross section for both colliders as well as providing simulated events for pp collisions at LHC.

In chapter 2, basic elements of the Standard Model are outlined according to the current understanding. Quantum Chromodynamics (QCD) is introduced as a theory describing the strong interaction and serves as an example for a non-Abelian gauge theory. Furthermore, a subset of the QCD-Feynman rules is derived as a tool to calculate cross sections. In chapter 3, the specific tree level Feynman diagrams belonging to $t\bar{t}$ production are evaluated. Moreover, the introduction of Faddeev-Popov ghost fields is motivated and three different methods for the calculation of the spin-averaged transition probability are presented before proceeding to the hadronic cross section. In chapter 4, the numerical methods of Monte Carlo integration as well as importance sampling are explained in order to compute the hadronic cross section. The results are then compared with the ones generated by the program TOP++ [4]. Finally, a basic Monte Carlo event generator is presented and the results achieved are discussed.

Notation

The Einstein summation convention is employed throughout this thesis. The complex conjugate is indicated via an asterisk $*$ whereas a bar $\overline{}$ on a fermion field represents the Dirac adjoint. The $(+, -, -, -)$ signature of the metric tensor $g_{\mu\mu}$ is used. The "Feynman slash notation"

$$\slashed{p} = \gamma_\mu p^\mu$$

is used as a shorthand for the inner product between a four-vector p and the Dirac gamma matrices γ^μ. The functions δ_{ab} and $\delta(x)$ denote the Kronecker symbol and the Dirac delta distribution. Physical quantities are expressed in natural units, i.e. $c = 1$ and $\hbar = 1$. An arrow $\vec{}$ distinguishes between a four-vector a and a three component vector $\vec{a}$.

The following are used:

$\sim$ rough correspondence

$\approx$ approximately equal

$:=$ defined as

$\overset{!}{=}$ this equal sign must be true

2 Gauge symmetries and path to QCD-Feynman rules

2.1 The Standard Model

The Standard Model (SM) of particle physics describes three of the four fundamental forces in the universe (the electromagnetic, weak and strong interaction except for gravitation) as well as all known elementary particles. The forces are mediated by gauge bosons, particles carrying an integer spin. Besides the bosons, the SM particles are made up of six quarks and six leptons. These particles belong to the group of fermions, particles with halfinteger spin following Fermi-Dirac statistics. All particles are depicted in fig. 2.1. To each particle there exists an anti-particle carrying opposite charge.

While all fermions take part in the weak interaction and all charged particles in the electromagnetic, the quarks are the only ones, apart from gluons, taking part in the strong interaction due to their property of carrying color charge. The theory describing the strong interaction is Quantum Chromodynamics. The name is inspired by additive color mixing, since the quarks can carry red, green or blue color charge. Unlike the the force carrier of electromagnetism, the gluons carry color charge as well and thus self interact. Each of the eight possible gluon states is connected to a color and anticolor. In line with the three basic colors, which mix together to form white, quarks also form a bound colorless state. This phenomenon, that so far in no experiment an individual free quark could be observed directly, is called confinement. In fact, this is because the strength of the interaction increases linearly with greater distances.

However, the coupling constant describing the strength of the interaction is actually dependent on the energy scale μ_R a process takes place at and decreases with increasing energy. This behavior is called asymptotic freedom and allows the application of perturbation theory in QCD (pQCD) at high enough energies. The scale dependence is also referred to as running coupling and is shown in fig. 2.1b. Mathematically, each of the interactions follows from the principle of gauge symmetry, i.e. each force is assigned to a gauge group and supposed to be invariant under this group. For example, the Lie group $U(1)$ is assigned to electromagnetism and the group $SU(2)$ to the weak interaction.
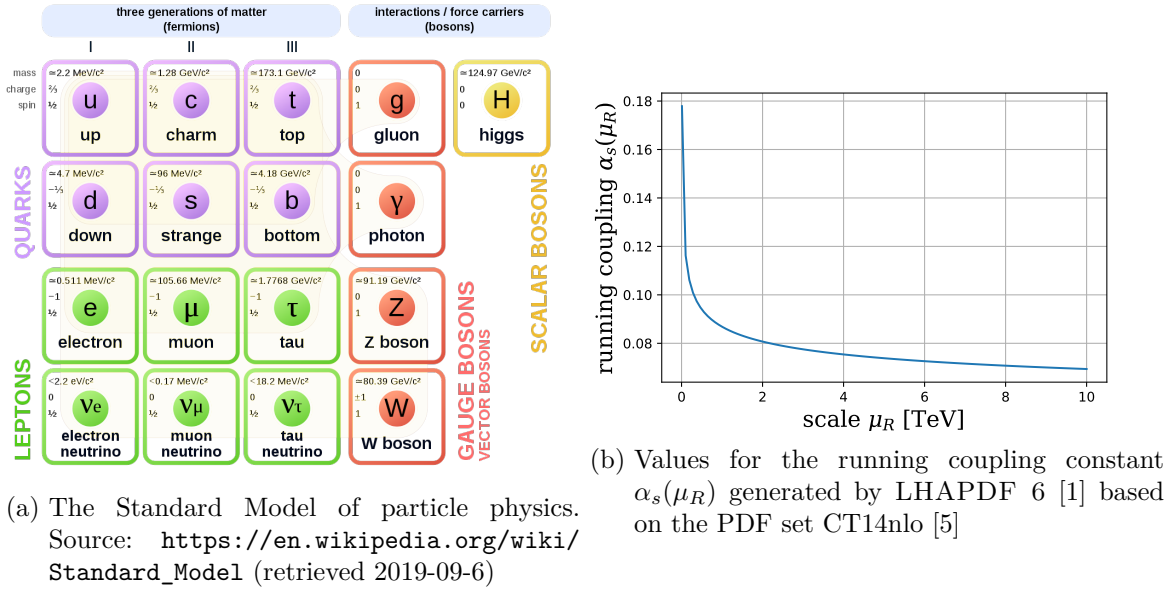
(a) The Standard Model of particle physics. Source: `https://en.wikipedia.org/wiki/Standard_Model` (retrieved 2019-09-6)

(b) Values for the running coupling constant $\alpha_s(\mu_R)$ generated by LHAPDF 6 [1] based on the PDF set CT14nlo [5]

Figure 2.1: The Standard Model and scale dependence of the strong coupling constant α_s

2.2 Symmetries and Quantum Chromodynamics

In quantum theory, a symmetry operation U leaves the measurable outcome of a system $|\Psi\rangle$ invariant. Of course, the normalization of the state must be conserved as well. This translates to the fact, that U must be a unitary operator:

$$\langle\Psi|\Psi\rangle = \langle\Psi| \, U^\dagger U \, |\Psi\rangle = \langle\Psi| \, \mathbb{1} \, |\Psi\rangle \, . \tag{2.1}$$

Moreover, symmetry operations form a group since there exists an inverse transformation (the adjoint operator in this case) and an identity element. In addition, two symmetry transformations carried out one after the other form a symmetry operation again. For this reason, especially Lie groups are of physical interest.

2.2.1 Lie algebras and Lie groups

This section is based on [12, chapter. 25.1]. A Lie group is a continuous group and also a differentiable manifold. Any group element can be written as

$$U = e^{i\theta_a T_a} \tag{2.2}$$

where T_a are known as the generators of a Lie group forming a Lie algebra and θ is a real constant. Requiring U to be unitary results in the fact that T_a must be Hermitian:

$$UU^\dagger = \exp\left(i\theta\left(T_a - T_a^\dagger\right)\right) \overset{!}{=} \mathbb{1}. \tag{2.3}$$

The Lie algebra is defined through the commutation relation

$$[T_a, T_b] = if_{abc}T_c \tag{2.4}$$

where f_{abc} are called structure constants and are completely antisymmetric in all indices. Moreover, the generators must satisfy the Jacobi identity

$$[T_a, [T_b, T_c]] + [T_b, [T_c, T_a]] + [T_c, [T_a, T_b]] = 0. \tag{2.5}$$

An example of a Lie group is the group $SU(2)$ used to describe the spin of fermions. However, for calculations in QCD the group $SU(3)$ is of special interest. In particular, the Casimirs for $SU(3)$ are $C_A = 3$, $T_R = \frac{1}{2}$ and $C_F = \frac{4}{3}$. The generators of $SU(3)$ in the fundamental representation $T_a = \frac{\lambda_a}{2}$ are identified with the Gell-Mann matrices.

$$\lambda_1 = \begin{pmatrix} 0 & 1 & 0 \\ 1 & 0 & 0 \\ 0 & 0 & 0 \end{pmatrix}, \lambda_2 = \begin{pmatrix} 0 & 0 & 1 \\ 0 & 0 & 0 \\ 1 & 0 & 0 \end{pmatrix}, \lambda_3 = \begin{pmatrix} 0 & 0 & 0 \\ 0 & 0 & 1 \\ 0 & 1 & 0 \end{pmatrix}, \lambda_4 = \begin{pmatrix} 0 & -i & 0 \\ i & 0 & 0 \\ 0 & 0 & 0 \end{pmatrix},$$

$$\lambda_5 = \begin{pmatrix} 0 & 0 & -i \\ 0 & 0 & 0 \\ i & 0 & 0 \end{pmatrix}, \lambda_6 = \begin{pmatrix} 0 & 0 & 0 \\ 0 & 0 & -i \\ 0 & i & 0 \end{pmatrix}, \lambda_7 = \begin{pmatrix} 1 & 0 & 0 \\ 0 & -1 & 0 \\ 0 & 0 & 0 \end{pmatrix}, \lambda_8 = \begin{pmatrix} \frac{1}{\sqrt{3}} & 0 & 0 \\ 0 & \frac{1}{\sqrt{3}} & 0 \\ 0 & 0 & -\frac{2}{\sqrt{3}} \end{pmatrix}$$

$$\tag{2.6}$$

.These matrices are normalized through the convention

$$f_{acd}f_{bcd} = C_A\delta_{ab}. \tag{2.7}$$

This implies the trace orthonormality

$$\mathrm{Tr}(T_a T_b) = T_R\delta_{ab}. \tag{2.8}$$

The following identities given in [11, appendix A.3] or [13, p. 7] are very useful for calculations in QCD as well

$$(T_a)_{ij}(T_a)_{kl} = T_R\left(\delta_{jk}\delta_{il} - \frac{1}{N}\delta_{ij}\delta_{kl}\right) \tag{2.9}$$

$$f_{abc}T_bT_c = \frac{1}{2}iC_AT_a. \tag{2.10}$$

2.2.2 Global gauge symmetry

The sections on gauge symmetries are based on [6, chapter 14]. A global symmetry is a symmetry where the parameter of the transformation θ is not dependent on space-time coordinates x. This means that a Lagrangian describing the field Ψ is invariant under the phase transformation

$$\Psi(x) \to e^{i\theta}\Psi(x). \tag{2.11}$$

where $e^{i\theta}$ is an element of the Abelian Lie group $U(1)$. For example, the Schrödinger equation is invariant under this transformation.

2.2.3 Local gauge symmetry and QCD

A stronger symmetry is a local transformation

$$\Psi(\vec{x}, t) \to e^{i\theta(x)}\Psi(\vec{x}, t) \tag{2.12}$$

where $\theta(x)$ now depends on space and time. The Lagrangian describing quarks and gluons can be derived by imposing this invariance on the Dirac Lagrangian

$$\mathcal{L}_{\mathrm{Dirac}} = \overline{\Psi}\left(i\gamma^\mu\partial_\mu - m\right)\Psi \tag{2.13}$$

but with the $SU(3)$ gauge group instead of $U(1)$

$$\Psi \to e^{i\theta_a(x)T_a}\Psi \tag{2.14}$$

and where the tensor γ_μ represents the gamma matrices fulfilling the anticommutation relation of a Clifford Algebra

$$\{\gamma^\nu, \gamma^\mu\} = 2g^{\mu\nu}. \tag{2.15}$$

The invariance is spoiled by the derivative

$$\partial_\mu e^{i\theta_a(x)T_a}\Psi(x) = e^{i\theta_a(x)T_a}\left(\partial_\mu\Psi(x) + iT_a\Psi(x)\partial_\mu\theta_a(x)\right). \tag{2.16}$$

This forces the introduction of eight gauge fields G_μ^a transforming as

$$G_\mu^a \to G_\mu^a - \frac{1}{g_s}\partial_\mu\theta_a(x) \tag{2.17}$$

to cancel the additional term in eq. (2.16). Then, the QCD Lagrangian becomes

$$\mathcal{L}_{\mathrm{QCD}} = \overline{\Psi}\left(i\gamma^\mu\partial_\mu - m\right)\Psi - g_s\left(\overline{\Psi}\gamma^\mu T_a\Psi\right)G_\mu^a. \tag{2.18}$$

However, since the generators T_a do not commute, the new term in eq. (2.18) breaks the invariance. Therefore, the gauge field must transform as

$$G_\mu^a \to G_\mu^a - \frac{1}{g_s}\partial_\mu\theta_a(x) - f_{abc}\theta_b(x)G_\mu^c. \tag{2.19}$$

Hence, one arrives at the final gauge invariant QCD Lagrangian

$$\mathcal{L}_{\text{QCD}} = \overline{\Psi}_j \left(i\gamma^\mu\partial_\mu - m\right)\Psi_i\delta_{ij} - g_s\left(\overline{\Psi}_i\gamma^\mu T_a\Psi_j\right)G_\mu^a - \frac{1}{4}G_{\mu\nu}^a G_a^{\mu\nu} \tag{2.20}$$

where the gluon field strength tensor reads as

$$G_{\mu\nu}^a = \partial_\mu G_\nu^a - \partial_\nu G_\mu^a - g_s f_{abc}G_\mu^b G_\nu^c \tag{2.21}$$

and contains an additional term compared to its counterpart in Quantum Electrodynamics (QED) allowing the self-interaction of gluons due to the non-Abelian gauge transformation. The indices i and j denote the color of the quark states[1].

2.2.4 QCD-Feynman rules

The rigorous approach to particle physics is quantum field theory. Within this framework there exist several formalisms to describe scattering processes, for example the Feynman path integral formalism or the Lagrangian approach. All methods lead to the same rules for describing such processes as well as the associated pictographic representations. These are called Feynman rules and Feynman diagrams. However, it is possible to obtain the same results using basic quantum theoretical knowledge even if some subtleties have to be overlooked.

In general, the transition amplitude T_{fi} for the scattering of an initial state $|\Phi_i\rangle$ to a final state $|\Phi_f\rangle$ due to an interaction H_{int} can be determined using time-dependent perturbation theory [2] given that the coupling of the interaction is small

$$\begin{aligned}
T_{fi} &= \langle\Phi_f|\,U(-\infty,\infty)\,|\Phi_i\rangle = \langle\Phi_f|\exp\left(-i\int_{-\infty}^{\infty}dt\;U^\dagger H_{\text{int}}U\right)|\Phi_i\rangle \\
&= \langle\Phi_f|\Phi_i\rangle - i\int_{-\infty}^{\infty}dt\;\langle\Phi_f|\,H_{\text{int}}\,|\Phi_i\rangle\,e^{-i(E_i-E_f)t} + ... \\
&\approx -i\delta(E_i - E_f)\,\langle\Phi_f|\,H_{\text{int}}\,|\Phi_i\rangle
\end{aligned} \tag{2.22}$$

where U is the time evolution operator. The states $|\Phi_f\rangle$ and $|\Phi_i\rangle$ are assumed to be orthogonal and have the same energies $E_f = E_i$. This approach can also be applied to the description of

---

[1] In chapter 3, these indices are expressed using three component color vectors c to allow the separation of the calculation in a Dirac and color trace in a more beautiful way.

[2] and the Dyson series

scattering processes in the strong interaction. Therefore it makes sense to separate the QCD Lagrangian into a free (non-interacting) part $\mathcal{L}_0$ and an interaction part $\mathcal{L}_{\text{int}}$. The kinetic part is given through the terms quadratic in fields.

$$\mathcal{L}_0 = \overline{q}_j \left(i\gamma^\mu \partial_\mu - m\right) q_i \delta_{ij} + \frac{1}{2}\partial_\mu G^a_\nu \partial^\mu G^\nu_a - \frac{1}{2}\partial_\mu G^a_\nu \partial^\nu G^\mu_a$$

$$\mathcal{L}_{\text{int}} = \underbrace{-g_s \overline{q}_i \gamma^\mu T_a q_j G^a_\mu}_{\mathcal{H}_{qqg}} \underbrace{- \frac{g_s f_{abc}}{4}\left(\partial_\mu G^a_\nu G^\mu_b G^\nu_c - \partial_\nu G^a_\mu G^\mu_b G^\nu_c - \partial_\mu G^b_\mu G^c_\nu G^\nu_a + \partial^\nu G^b_\mu G^c_\nu G^\mu_a\right)}_{\mathcal{H}_{3g}}$$

$$+ \underbrace{g_s^2 f_{abc} f_{abc} \frac{1}{4} G^b_\mu G^c_\nu G^\mu_b G^\nu_c}_{\mathcal{H}_{4g}} \tag{2.23}$$

The four-gluon interaction $\mathcal{H}_{4g}$ shall be excluded from the following considerations since the relevant interaction terms for quark pair-production are the quark-gluon and triple-gluon interaction. These terms contain three fields. Two of them can be identified with the initial and final particle states whereas the remaining terms represent the interaction H_{int}. This means that the third field being part of H_{int} is the cause of the scattering which, in turn, is generated by other particles. To examine this fact, each of the three possible configurations of the initial and final particle states is considered, i.e. quark and quark, gluon and quark as well as gluon and gluon. In the first case, the initial and final particles shall be given by two quarks q_1 and q_2

$$\langle q_1| - g_s \gamma^\mu T_a G^a_\mu |q_2\rangle \quad \text{or} \quad \langle q_2| - g_s \gamma^\mu T_a G^a_\mu |q_1\rangle \tag{2.24}$$

scattering off a potential created by the quarks q_3 and q_4 mediated through G^a_μ. The gluon field G^a_μ can now be determined by solving the equation of motion for a free gluon perturbed by q_3 and q_4. The equation of motion follows from the Euler-Lagrange equation

$$\partial_\mu \frac{\partial \mathcal{L}_0}{\partial \left(\partial_\mu G^a_\nu\right)} - \frac{\partial \mathcal{L}_0}{\partial G^a_\nu} = 0 \tag{2.25}$$

and yields including the perturbation

$$\partial_\mu \partial^\mu G^\nu_a - \partial_\mu \partial^\nu G^\mu_a = -g_s \overline{q}_{3/4} \gamma^\nu T_a q_{4/3} =: j^\nu_{34} \tag{2.26}$$

or in momentum space $(i\partial_\mu \to q_\mu)$

$$\left(-q^2 g_\mu{}^\nu + q_\mu q^\nu\right) G^\nu_a = j^\nu_{34}. \tag{2.27}$$

However, the operator on the left cannot be inverted due to the fact that the eigenvalue to the eigenvector p^μ is zero which is a manifestation of gauge invariance as several choices of the gluon field represent the same physics residing in j^ν_{34}. Therefore it is necessary to fix the

gauge. This is done by adding an auxiliary field $\frac{1}{2\xi}\left(G_\mu^a G_a^\mu\right)^2$ to $\mathcal{L}_0$ acting like a Lagrange multiplier. As a consequence, the equation to be solved becomes

$$\left(-q^2 g_\mu{}^\nu + \left(1 - \frac{1}{\xi}\right) q_\mu q^\nu\right) G_a^\nu = j_{34}^\nu \tag{2.28}$$

and the inverted operator called the gluon propagator yields

$$\Pi_{\mu\nu} = -\frac{g_{\mu\nu} - (1 - \xi)\frac{q_\nu q_\mu}{q^2}}{q^2}. \tag{2.29}$$

Since the final result for the transition probability should not depend on the choice of ξ it is most convenient to work in Feynman gauge $\xi = 1$. If now the momenta p_1, p_2, p_3 and p_4, the spins s_1, s_2, s_3 and s_4 as well as the colors i, j k and l are assigned to the quarks while the quark states are expressed through Dirac spinors[3] and color vectors

$$c_1 = \begin{pmatrix} 1 \\ 0 \\ 0 \end{pmatrix}, \qquad c_2 = \begin{pmatrix} 0 \\ 1 \\ 0 \end{pmatrix}, \qquad c_3 = \begin{pmatrix} 0 \\ 0 \\ 1 \end{pmatrix}, \tag{2.30}$$

one has accomplished to find an expression for the transition amplitude for the scattering processes sketched in fig. 2.2

$$
\begin{aligned}
T_{fi}^{(a)} &= -\int dx^4 \overline{u}(p_2, s_2) c_i^\dagger e^{ip_2 x} \left(-g_s \gamma^\mu T_a\right) u(p_1, s_1) c_j e^{-ip_1 x} \frac{-ig_{\mu\nu}}{(p_2 - p_1)^2} \\
&\quad \times \overline{u}(p_4, s_4) c_k^\dagger e^{ip_4 x} \left(-g_s \gamma^\nu T_a\right) u(p_3, s_3) c_l e^{-ip_3 x} \\
&= \delta^{(4)}(p_2 + p_4 - p_1 - p_3) \overline{u}(p_2, s_2) c_i^\dagger \left(-ig_s \gamma^\mu T_a\right) u(p_1, s_1) c_l \frac{-ig_{\mu\nu}}{(p_2 - p_1)^2} \\
&\quad \times \overline{u}(p_4, s_4) c_k^\dagger \left(-ig_s \gamma^\nu T_a\right) u(p_3, s_3) c_l =: \delta^{(4)}(p_2 + p_4 - p_1 - p_3)\left(-i\mathfrak{M}\right) \\
T_{fi}^{(b)} &= \delta^{(4)}(p_2 + p_4 - p_1 - p_3) \overline{v}(p_2, s_2) c_i^\dagger \left(-ig_s \gamma^\mu T_a\right) u(p_1, s_1) c_j \frac{-ig_{\mu\nu}}{(p_1 + p_2)^2} \\
&\quad \times \overline{u}(p_4, s_4) c_k^\dagger \left(-ig_s \gamma^\nu T_a\right) v(p_3, s_3) c_l
\end{aligned} \tag{2.31}
$$

where $-i\mathfrak{M}$ is called the invariant amplitude. The delta function ensures moment conservation and is included in the Lorentz invariant phase space factor $d\Pi_{\text{Lips}}$ covered in the next chapter. In the course of the considerations the quark gluon vertex[4] was derived

---

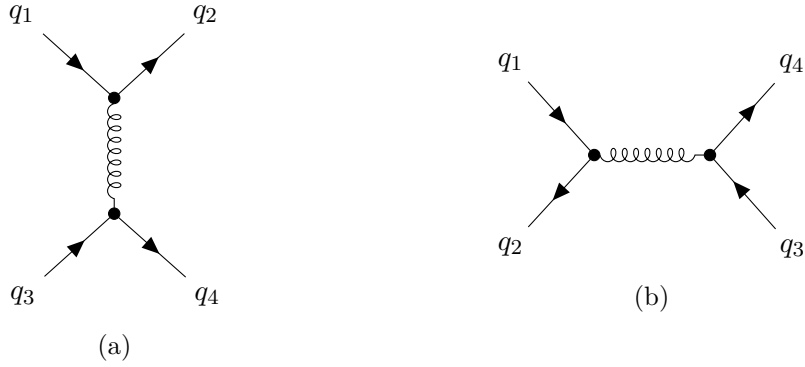[3] u and $\overline{u}$ for fermions and v and $\overline{v}$ for antifermions

Figure 2.2: Feynman diagrams for quark-quark scattering and quark pair production. Time flows from left to right.

$$= -ig_s\gamma_\mu T_a \tag{2.32}$$

as well as the gluon propagator

$$= \frac{-ig_{\mu\nu}}{q^2}. \tag{2.33}$$

The additional i originates from the time evolution operator. The same gluon propagator is obtained when assuming two gluons in the initial and final state as well as changing the perturbation in eq. (2.27) to a triple-gluon one. However, these assumptions result in two major changes in the transition amplitude. The particle states of gluons do not correspond to solutions of the Dirac equation but must be determined from the equation of motion for a free gluon (after setting $\xi = 1$)

$$\partial^\nu \partial_\nu G_\mu^a = 0 \tag{2.34}$$

which can be solved by
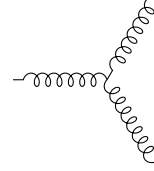
$$G_\mu^a = \epsilon_\mu^a(k)e^{-ikx} \tag{2.35}$$

where the four-vector $\epsilon_\mu(k)$ is referred to as the polarization vector of a gluon [5]. The second change relates to the replacement of the quark-gluon vertex with the triple-gluon vertex contained in $\mathcal{H}_{3g}$. The terms proportional to G^3 can be simplified to

$$- g_s f_{abc}\partial^\nu G_\nu^b G_\mu^a G_c^\mu = -g_s f_{abc}g_{\mu\lambda}\partial^\nu G_\nu^b G_a^\lambda G_c^\mu \tag{2.36}$$

---

[4]A vertex corresponds to the coefficients of the fields in the interaction term.

[5]The color index on the polarization vector is omitted from now on.

by invoking the antisymmetric property of the structure constants. Summing over the 3! possible orderings of gluons and Fourier transforming to momentum space gives the triple-gluon vertex

$$= g_s f_{abc} \left(g_{\mu\nu}(p_1 - p_2)_\lambda + g_{\nu\lambda}(p_2 - p_3)_\mu + g_{\lambda\mu}(p_3 - p_1)_\nu \right) \tag{2.37}$$
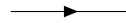
The last combination of initial and final fields to be examined is given by a quark and a gluon. This means the remaining field in $\mathcal{H}_{qqg}$ is a quark field. It can be determined similar to the gluon propagator by solving the equation

$$(i\gamma^\mu \partial_\mu - m)\, q = -g_s \gamma^\mu T_b G^a_\mu q. \tag{2.38}$$

or in momentum space

$$\left(\slashed{q} - m \right) q = -g_s \gamma^\mu T_b G^a_\mu q. \tag{2.39}$$

In other words, the quark propagator
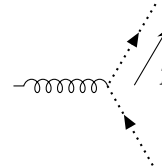
$$= \frac{i}{\slashed{q} - m} = \frac{i \left(\slashed{q} + m \right)}{\left(\slashed{q} - m \right)\left(\slashed{q} + m \right)} = \frac{i \left(\slashed{q} + m \right)}{q^2 - m^2}. \tag{2.40}$$

is given by the inverse of the Schrödinger operator on the left-hand side. The following relation proofed to be helpful in the derivation of the quark propagator

$$\slashed{q}\slashed{q} = \frac{1}{2} q_\nu q_\mu \{\gamma^\nu, \gamma^\mu\} \overset{2.15}{=} g^{\mu\nu} q_\nu q_\mu = q^2. \tag{2.41}$$

The last ingredient for the description of quark production is the ghost vertex

$$p \quad = -g_s f_{abc} p^\mu \tag{2.42}$$

which shall not be derived here. However, a motivation for the introduction of this scalar field is given in the next chapter. The complete set of QCD-Feynman rules can be found in [12, chapter 26.1] or [11, appendix A.1].

3 Top quark pair-production at leading order

Experimentally, top quarks are produced in high-energy $p\overline{p}$ collisions at Tevatron or in pp collisions at LHC. The production process takes place predominantly via the strong interaction. Of course, a $t\bar{t}$ pair can be created through the decay of a Z boson or a QED process as well, but their contributions are negligible due to the comparably low coupling constants of the weak and electromagnetic interaction at the TeV-scale. For that reason, only QCD processes are considered in this work. Since the strong coupling constant takes small values for scales $\mu_R \sim m_t = (173.29 \pm 0.95)\,\text{GeV}$ [3, p. 11] (see fig. 2.1b), accurate predictions for $t\bar{t}$ production can be obtained by using perturbative QCD in g_s as outlined before. During this calculation all quark masses m_q other than the top mass are considered negligible.

3.1 Kinematics

In most hadron colliders, the particle beams are directed into each other with opposite momenta to ensure that all their energy contributes to the collision. Since hadrons are no elementary particles, the collisions at high enough energies take place between their constituent quarks and gluons, the so-called partons. Therefore, it is useful to define the momenta in the interacting partons' center-of-mass system. Let k and k' be the four-momenta of the incoming partons with energy E and p and p' the ones of the outgoing quarks where the direction of acceleration is given by the z-axis

$$k = E \begin{pmatrix} 1 \\ \vec{e_z} \end{pmatrix} \qquad\qquad k' = E \begin{pmatrix} 1 \\ -\vec{e_z} \end{pmatrix}$$

$$p = \begin{pmatrix} E \\ \begin{pmatrix} \sin(\theta) \\ 0 \\ \cos(\theta) \end{pmatrix} \sqrt{E^2 - m_t^2} \end{pmatrix} \qquad p' = \begin{pmatrix} E \\ \begin{pmatrix} -\sin(\theta) \\ 0 \\ -\cos(\theta) \end{pmatrix} \sqrt{E^2 - m_t^2} \end{pmatrix}. \tag{3.1}$$

One disadvantage of this definition is, that the momenta in the laboratory frame where the detectors are placed in is no longer identical to those in the center-of-mass frame of the

partons. However, a momentum p^{CMS} can be transformed into the lab frame via a Lorentz boost along the z-direction

$$
p^{\mathrm{lab}} = \begin{pmatrix} \gamma p_0^{\mathrm{CMS}} - \gamma\beta p_3^{\mathrm{CMS}} \\ p_1^{\mathrm{CMS}} \\ p_2^{\mathrm{CMS}} \\ -\gamma\beta p_0^{\mathrm{CMS}} + \gamma p_3^{\mathrm{CMS}} \end{pmatrix} \tag{3.2}
$$

where γ is the Lorentz factor (cf. [10, p. 15]). The distribution in the angle φ is isotropic for a $2 \to 2$ process, that's why the angle is not included in the definition of the momenta in eq. (3.1). Usually, it is handy to describe the scattering process in terms of the Lorentz invariant Mandelstam variables

$$
\begin{aligned}
s &:= \left(k + k'\right)^2 = \left(p + p'\right)^2 = 2k \cdot k' = 2p \cdot p' + 2m_t^2 \\
t &:= \left(k - p\right)^2 = \left(p' - k'\right)^2 = -2k \cdot p + m_t^2 = -k' \cdot p' + 2m_t^2 \\
u &:= \left(k - p'\right)^2 = \left(k' - p\right)^2 = -k \cdot p' + m_t^2 = -k' \cdot p + m_t^2
\end{aligned} \tag{3.3}
$$

where $\sqrt{s} = 2E$ is the center-of-mass energy. The Mandelstam variables are related through

$$
s + t + u = 2m_t^2 \tag{3.4}
$$

due to momentum conservation.

3.2 Production processes

In order to describe top quark pair-production at tree level, one has to consider all Feynman diagrams proportional to g_s^2 and result in a $t\bar{t}$-pair in the final state on the basis of the QCD-Feynman rules. At this order, two processes gg-fusion and $q\bar{q}$-annihilation contribute to the transition amplitude. The corresponding Feynman diagrams are displayed in fig. 3.1. In these diagrams time flows from left to right. In fig. 3.1b the fist two diagrams differ only by the exchange of the outgoing quarks. The incoming gluons could have been interchanged as well.

3.3 Calculation of the square invariant amplitude

Since all quarks other than the top are considered massless, the first diagram is suitable to give a more detailed account on how a Feynman diagram and its square amplitude are
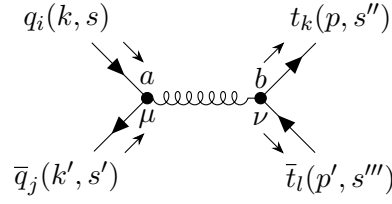
(a) Diagram for $q\bar{q}$-annihilation. The variables assigned to four-momenta, spins, colors and vertices are explicitly labeled.
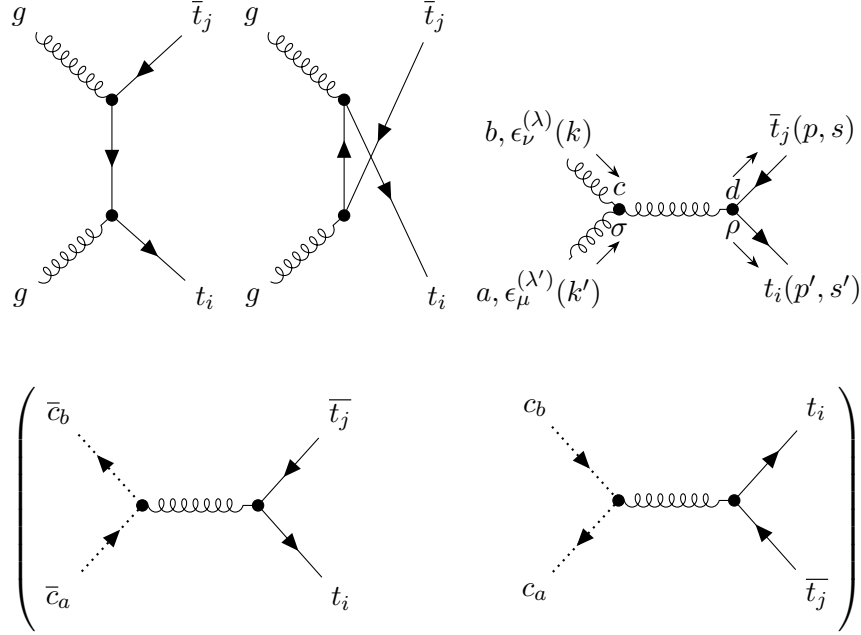
(b) Diagrams for the the gluon fusion process. Whether the ghost diagrams are to be included depends on the applied polarization sum during the calculation of the spin summed and averaged square amplitude.

Figure 3.1: Tree level Feynman diagrams contributing to $t\bar{t}$ production. Cf. [9, p. 2]

evaluated. In general, calculations of square matrix elements in QCD can be subdivided into the evaluation of a color and Dirac trace. This is expressed using the proportional sign.

3.3.1 Quark-antiquark annihilation

Following the two separate fermion lines and applying the QCD-Feynman rules from section 2.2.4 one can immediately write down the corresponding amplitude[1]

$$ -i\mathfrak{M}_{q\bar{q}} = \overline{v}(k',s')c_j^\dagger \left(-ig_s\gamma^\mu T_a\right) u(k,s)c_i \frac{-ig_{\mu\nu}\delta_{ab}}{(k+k')^2}\overline{u}(p,s'')c_k^\dagger \left(-ig_s\gamma^\nu T_b\right) v(p',s''')c_l. \quad (3.5) $$

---

[1]This transition amplitude has already been explicitly derived using perturbation theory in eq. (2.31).

Since the goal is the square amplitude, it is useful to calculate its adjoint by exploiting the properties of γ-matrices given in [6, chapter 5] as well as that T_a is Hermitian for $SU(N)$.

$$
\begin{aligned}
i\mathfrak{M}^\dagger{}_{q\bar{q}} &= -ig_s^2 c_l^\dagger v^\dagger(p',s''') (\gamma^\sigma)^\dagger T_b^\dagger \left(c_k^\dagger\right)^\dagger \overline{u}^\dagger(p,s'') \frac{g_{\sigma\lambda}\delta_{ab}}{s} c_i^\dagger u^\dagger(k,s) \left(\gamma^\lambda\right)^\dagger T_a^\dagger \left(c_j^\dagger\right)^\dagger \overline{v}^\dagger(k',s') \\
&= -ig_s^2 c_l^\dagger v^\dagger(p',s''') \gamma^0 \gamma^\sigma \gamma^0 T_b c_k \gamma^0 u(p,s'') \frac{g_{\sigma\lambda}\delta_{ab}}{s} c_i^\dagger u^\dagger(k,s) \gamma^0 \gamma^\lambda \gamma^0 T_a c_j \gamma^0 v(k',s') \quad (3.6) \\
&= -i\frac{g_s^2 \delta_{ab}}{s} (T_b)_{lk} (T_a)_{ij} \overline{v}(p',s''')\gamma^\sigma u(p,s'')\overline{u}(k,s)\gamma^\lambda v(k',s')
\end{aligned}
$$

Since color charge is not detectable, all initial color states are averaged and all final states are summed. It makes sense to perform the computations of the color factor for a general $SU(N)$ gauge theory and set $N=3$ at the end of the calculation.

$$
\begin{aligned}
\frac{1}{N^2}\sum_{i,j,k,l,a,b} |\mathfrak{M}_{q\bar{q}}|^2 &\propto \frac{c_j^\dagger T_a c_i c_k^\dagger T_b c_l c_l^\dagger T_b^\dagger c_k c_i^\dagger T_a^\dagger c_j \delta_{ab}}{N^2} = \frac{(T_a)_{ji}(T_b)_{kl}(T_b)_{lk}(T_a)_{ij}\delta_{ab}}{N^2} \\
&= \frac{\text{Tr}(T_a T_a)^2}{N^2} \overset{2.8}{=} \frac{T_R^2}{N^2}\delta_{aa} = \frac{T_R^2}{N^2}(N^2-1) = \frac{2T_R^2 C_F}{N}
\end{aligned}
\tag{3.7}
$$

Averaging over spins of the initial particles and summing over the spins of the outgoing top quarks using the completeness relations [6, p. 111]

$$
\sum_s u(p,s)\overline{u}(p,s) = \slashed{p} + m \tag{3.8}
$$

$$
\sum_s v(p,s)\overline{v}(p,s) = \slashed{p} - m \tag{3.9}
$$

as well as employing the trace theorems listed in [12, appendix A.4] to obtain the unpolarized transition probability yields

$$
\begin{aligned}
\frac{1}{4}\sum_{s,s',s'',s'''} |\mathfrak{M}_{q\bar{q}}|^2 &\propto \frac{1}{4}\text{Tr}(\slashed{k}'\gamma^\mu \slashed{k}\gamma^\lambda)\text{Tr}((\slashed{p}+m_t)\gamma_\mu(\slashed{p}'-m_t)\gamma_\lambda) \\
&= \frac{1}{4}k'_\alpha k_\beta \text{Tr}(\gamma^\alpha \gamma^\mu \gamma^\beta \gamma^\lambda)(-m_t^2 \text{Tr}(\gamma_\mu\gamma_\lambda) + p^\alpha p'^\beta \text{Tr}(\gamma_\alpha\gamma_\mu\gamma_\beta\gamma_\lambda)) \\
&= k'_\alpha k_\beta (g^{\alpha\mu}g^{\beta\lambda} - g^{\alpha\beta}g^{\mu\lambda} + g^{\alpha\lambda}g^{\mu\beta}) \\
&\quad \times (-4m_t g_{\mu\lambda} + 4p^\alpha p'^\beta(g_{\alpha\mu}g_{\beta\lambda} - g_{\alpha\beta}g_{\mu\lambda} + g_{\alpha\lambda}g_{\mu\beta})) \\
&= (k'^\mu k^\lambda - (k'\cdot k)g^{\mu\lambda} + k'^\lambda k^\mu)(4m_t^2 g_{\mu\lambda} + 4(p_\mu p'_\lambda - (p\cdot p')g_{\mu\lambda}) + p_\lambda p'_\mu) \\
&= 8m_t^2(k\cdot k') + 8(p\cdot k')(p'\cdot k) + 8(k'\cdot p')(k\cdot p)
\end{aligned}
\tag{3.10}
$$

This expression can be simplified further by rewriting everything in terms of the Mandelstam variables s, t and u defined in eq. (3.3). Then, the final result for the averaged and summed square invariant amplitude for $q\bar{q}$-annihilation at leading order is

$$\overline{|\mathfrak{M}_{q\bar{q}}|^2} = \frac{g_s^4}{s^2} \frac{T_R^2 C_F}{N} (2m_t^4 + u^2 + t^2 + 2m_t^2(s - u - t)) \tag{3.11}$$

3.3.2 Gluon fusion

The amplitudes for gg-fusion according to the Feynman rules are

$$-i\mathfrak{M}_1 = \overline{u}(p', s')c_i^\dagger (-ig_s\gamma^\mu T_a) \frac{i(\not{p}' - \not{k}' + m_t)}{(p' - k')^2 - m_t^2} (-ig_s\gamma^\nu T_b) \overline{v}(p, s)c_j \epsilon_\nu^{(\lambda)}(k)\epsilon_\mu^{(\lambda')}(k') \tag{3.12}$$

$$-i\mathfrak{M}_2 = \overline{u}(p', s')c_i^\dagger (-ig_s\gamma^\nu T_b) \frac{i(\not{k}' - \not{p} + m_t)}{(k' - p)^2 - m_t^2} (-ig_s\gamma^\mu T_a) \overline{v}(p, s)c_j \epsilon_\nu^{(\lambda)}(k)\epsilon_\mu^{(\lambda')}(k') \tag{3.13}$$

$$-i\mathfrak{M}_3 = \overline{u}(p', s')c_i^\dagger (-ig_s\gamma_\rho T_d) \overline{v}(p, s)c_j \frac{-ig^{\rho\sigma}\delta_{cd}}{(k + k')^2}(-gf_{abc})\mathcal{M}^{\nu\mu}{}_\sigma \epsilon_\nu^{(\lambda)}(k)\epsilon_\mu^{(\lambda')}(k'). \tag{3.14}$$

The shorthand

$$\mathcal{M}^{\nu\mu}{}_\sigma = g^\nu{}_\sigma(2k' + k)^\mu + g^{\nu\mu}(k' - k)_\sigma + g^\mu{}_\sigma(-2k' - k)^\nu \tag{3.15}$$

will be useful. Whether the ghost diagrams are to be included in the calculation depends on how the nonzero probabilities to produce longitudinal polarization states are handled which is covered in great detail in the course of this section

$$-i\mathfrak{M}_{\text{ghost},1} = \overline{u}(p', s')c_i^\dagger (-ig_s\gamma_\rho T_d) v(p, s)c_j \frac{-ig_{\lambda\sigma}\delta_{cd}}{(k + k')^2} g_s f_{abc}(-k^\sigma)$$
$$-i\mathfrak{M}_{\text{ghost},2} = \overline{u}(p', s')c_i^\dagger (-ig_s\gamma_\rho T_d) v(p, s)c_j \frac{-ig_{\lambda\sigma}\delta_{cd}}{(k + k')^2} g_s f_{abc}(-k'^\sigma). \tag{3.16}$$

The total transition amplitude for one process is equal to the sum over all amplitudes of the subprocesses

$$\mathfrak{M}_{gg} = \mathfrak{M}_1 + \mathfrak{M}_2 + \mathfrak{M}_3. \tag{3.17}$$

The goal is the square matrix element which is given by [2]

$$|\mathfrak{M}_{gg}|^2 = |\mathfrak{M}_1|^2 + |\mathfrak{M}_2|^2 + |\mathfrak{M}_3|^2 + 2\text{Re}(\mathfrak{M}_1\mathfrak{M}_2^\dagger) + 2\text{Re}(\mathfrak{M}_1\mathfrak{M}_3^\dagger) + 2\text{Re}(\mathfrak{M}_2\mathfrak{M}_3^\dagger). \tag{3.18}$$

Before moving on to the discussion on polarization states and ghosts fields the color averaging shall be performed. This time the transition probability must be averaged over $(N^2 - 1)^2$

---

[2] Thanks to the relation $z_1 z_2^* - z_1^* z_2 = (x_1 + iy_1)(x_2 - iy_2) + (x_1 - iy_1)(x_2 + iy_2) = 2x_1 x_2 + 2y_1 y_2 = 2\text{Re}(z_1 z_2^*)$, where $z_1, z_2 \in \mathbb{C}$ and $x_1, x_2, y_1, y_2 \in \mathbb{R}$, one only needs to calculate half of the interference terms.

possible color combinations of the initial gluons, since a general gauge group $SU(N)$ possesses $N^2 - 1$ generators which correspond to the force-carrier.

$$\overline{|\mathfrak{M}_1|^2} \propto \frac{1}{(N^2-1)^2}(T_a)_{ij}(T_a)_{jk}(T_b)_{kl}(T_b)_{li}$$

$$\stackrel{2.9}{=} \frac{T_R^2}{(N^2-1)^2}(\delta_{ik}\delta_{jj} - \frac{1}{N}\delta_{ij}\delta_{jk})(\delta_{ki}\delta_{ll} - \frac{1}{N}\delta_{kl}\delta_{li}) \tag{3.19}$$

$$= T_R^2 \frac{N^4 - 2N^2 + 1}{N(N^2-1)^2} = \frac{T_R^2}{N}$$

$$\overline{|\mathfrak{M}_2|^2} \propto \frac{\text{Tr}(T_b T_a T_a T_b)}{(N^2-1)^2} \stackrel{3.19}{=} \frac{T_R^2}{N} \tag{3.20}$$

$$\overline{|\mathfrak{M}_3|^2} \propto \frac{(T_c)_{ij}(T_e)_{ji}f_{abc}f_{abc}}{(N^2-1)^2} \stackrel{2.7}{=} \frac{C_A}{(N^2-1)^2}\text{Tr}(T_c T_c)\delta_{cc} \stackrel{2.8}{=} \frac{T_R C_A}{N^2-1} \tag{3.21}$$

$$\overline{\mathfrak{M}_1 \mathfrak{M}_2^\dagger} \propto \frac{(T_a T_b)_{ij}(T_a T_b)_{ji}}{(N^2-1)^2} = \frac{1}{(N^2-1)^2}(T_a)_{ik}(T_a)_{jl}(T_b)_{kj}(T_b)_{li}$$

$$\stackrel{2.9}{=} \frac{T_R^2}{(N^2-1)^2}(\delta_{il}\delta_{kj} - \frac{1}{N}\delta_{ik}\delta_{jl})(\delta_{ki}\delta_{jl} - \frac{1}{N}\delta_{kj}\delta_{li}) \tag{3.22}$$

$$= T_R^2 \frac{1 - N^2}{N(N^2-1)^2} = \frac{-T_R^2}{N(N^2-1)}$$

$$\overline{\mathfrak{M}_1 \mathfrak{M}_3^\dagger} \propto \frac{-i(T_a T_b)_{ij}(T_c)_{ij}f_{abc}}{(N^2-1)^2} = \frac{-i\text{Tr}(T_a T_b T_c)f_{abc}}{(N^2-1)^2}$$

$$\stackrel{2.10}{=} \frac{C_A}{2(N^2-1)^2}\text{Tr}(T_a T_a) \stackrel{2.8}{=} \frac{C_A T_R}{2(N^2-1)} \tag{3.23}$$

$$\overline{\mathfrak{M}_2 \mathfrak{M}_3^\dagger} \propto \frac{-i(T_b T_a)_{ij}(T_c)_{ji}f_{abc}}{(N^2-1)^2} = \frac{-i\text{Tr}(T_b T_a T_c)f_{abc}}{(N^2-1)^2}$$

$$= \frac{-i\text{Tr}(T_b T_a T_c)(-f_{cba})}{(N^2-1)^2} \stackrel{3.23}{=} -\frac{C_A T_R}{2(N^2-1)} \tag{3.24}$$

In the interference terms with $\mathfrak{M}_3^\dagger$ occurs a factor $-i$ which is included in the color factor to ensure a real valued Dirac as well as color trace.

Ward identity and polarization states

While the evaluation of the color factors was straightforward, the calculation of the spin-averaged Dirac trace gets more complicated since the invariant Amplitude $\mathfrak{M}_1 + \mathfrak{M}_2 + \mathfrak{M}_3$ is no longer gauge invariant which becomes obvious by checking the Ward identity (cf. [11, chapter 16])

$$\mathfrak{M}_{gg} = \epsilon_\nu^{(\lambda)}(k)\epsilon_\mu^{(\lambda')}(k')M_{gg}^{\nu\mu} \qquad \rightarrow \qquad k_\nu M_{gg}^{\nu\mu} = k'_\mu M_{gg}^{\nu\mu} = 0. \tag{3.25}$$

Firstly, one has to examine

$$k_\nu \left(M_1^{\nu\mu} + M_2^{\nu\mu}\right) = g_s^2 \overline{u}(p', s')\left((\not{p}' - \not{k} + m_t)\not{k}\frac{(T_a T_b)_{ij}}{t - m_t^2} + \not{k}(\not{k}' - \not{p} + m_t)\frac{(T_b T_a)_{ij}}{u - m_t^2}\right)v(p, s)$$

$$= g_s^2 \overline{u}(p', s')(t - m_t^2 + \slashed{k}(\slashed{p} + m_t))\slashed{k}\frac{(T_a T_b)_{ij}}{t - m_t^2}v(p, s) \tag{3.26}$$

$$+ g_s^2 \overline{u}(p', s')\slashed{k}(m_t^2 - u - (\slashed{p}' - m_t)\slashed{k}))\frac{(T_b T_a)_{ij}}{u - m_t^2}v(p, s)$$

$$= ig_s^2 (T_c)_{ij} f_{abc}\overline{u}(p', s')\gamma^\mu v(p, s)\frac{2k'k}{s}$$

Then, the Mandelstam variables have to be introduced somehow.

$$(\slashed{p}' - \slashed{k}')\slashed{k} = (\slashed{k} - \slashed{p})\slashed{k} \stackrel{2.41}{=} -\slashed{p}\slashed{k} = -p_\nu k_\mu \gamma^\nu \gamma^\mu \stackrel{2.15}{=} -2p \cdot k + \slashed{k}\slashed{p} \stackrel{3.3}{=} t - m_t^2 + \slashed{k}\slashed{p}$$

$$\slashed{k}(\slashed{k}' - \slashed{p}) = \slashed{k}(\slashed{p}' - \slashed{k}) \stackrel{2.41}{=} -\slashed{p}\slashed{k} = m_t^2 - u + \slashed{k}\slashed{p} \tag{3.27}$$

The final expression in eq. (3.26) can be obtained by applying the Dirac equation

$$\overline{u}(p', s')(\slashed{p}' - m_t) = 0 \qquad\qquad (\slashed{p} + m_t)v(p, s) = 0 \tag{3.28}$$

and the commutator of the Gell-Mann matrices in eq. (2.4). The insertion of $\frac{2kk'}{s}$ which is in fact one makes sense when regarding the third transition amplitude

$$k_v M_3^{\nu\mu} = i\frac{g_s^2}{s}(T_c)_{ij} f_{abc}\overline{u}(p', s') \left(\gamma^\sigma k_\sigma(2k + k')^\mu + \gamma^\sigma k^\mu(k' - k)_\sigma - 2\gamma^\mu k' \cdot k\right) v(p, s). \tag{3.29}$$

The first two amplitudes precisely cancel the last term and since the calculation is performed in the quarks' center-of-mass frame, the expression in the brackets is reduced to

$$\gamma^\sigma(k_\sigma(2k + k')^\mu + k^\mu(k' - k)_\sigma) = \slashed{k}k'^\mu. \tag{3.30}$$

Combining eq. (3.26) and eq. (3.29) yields

$$k_\nu M_{gg}^{\nu\mu} = k^\mu i\frac{g_s^2}{s}(T_c)_{ij} f_{abc}\overline{u}(p', s')\slashed{k}'v(p, s) = k^\mu \mathfrak{M}_{\text{ghost},2}. \tag{3.31}$$

In the exact same manner one obtains

$$k'_\mu M_{gg}^{\nu\mu} = k'^\nu \mathfrak{M}_{\text{ghost},1}. \tag{3.32}$$

This implies that there is a nonvanishing amplitude to produce longitudinal gauge bosons. Thus, these unphysical polarization states cannot be omitted from QCD calculations although this is true for processes in QED due to the Ward identity. To account for this problem, one has to include so-called Faddeev-Popov ghosts. These "particles" cancel exactly the

contribution of longitudinal gluons which is motivated by eq. (3.31) and eq. (3.32). Therefore, one is allowed to employ the same replacement as in QED

$$\sum_{\lambda=L,R} \epsilon_\mu^{(\lambda)*}(k)\epsilon_\nu^{(\lambda)}(k) \rightarrow -g_{\mu\nu}. \tag{3.33}$$

Another approach is to explicitly include the unphysical polarization states in the summation process. These forward and backward lightlike polarization vectors parallel to the acceleration axis can be written as follows:

$$\begin{aligned}\epsilon^+(k) &= \frac{1}{\sqrt{2}|\vec{k}|}k \\ \epsilon^-(k') &= \frac{1}{\sqrt{2}|\vec{k'}|}k'.\end{aligned} \tag{3.34}$$

The transverse polarizations

$$\epsilon^1 = \begin{pmatrix} 0 \\ \vec{e}_x \end{pmatrix} \text{ and } \epsilon^2 = \begin{pmatrix} 0 \\ \vec{e}_y \end{pmatrix} \tag{3.35}$$

are orthogonal to k and k'. In order to cancel the square amplitudes for producing longitudinal states, the polarization vectors have to be inserted in the following way.

$$\begin{aligned}\overline{|\mathfrak{M}_{gg}|^2} &\propto M_{gg}^{\mu\nu} M_{gg}^{\dagger\alpha\beta} \left(-\epsilon_\mu^-(k')\epsilon_\alpha^{+*}(k) - \epsilon_\mu^+(k)\epsilon_\alpha^{-*}(k') + \epsilon_\mu^1\epsilon_\alpha^{1*} + \epsilon_\mu^2\epsilon_\alpha^{2*}\right)\left(\epsilon_\nu^1\epsilon_\beta^{1*} + \epsilon_\nu^2\epsilon_\beta^{2*}\right) \\ &= |M_{gg}^{11}|^2 + |M_{gg}^{22}|^2 - M_{gg}^{\mu 1}M_{gg}^{\dagger\alpha 1}\frac{k'_\mu k_\alpha + k_\mu k'_\alpha}{k\cdot k'} - M_{gg}^{\mu 2}M_{gg}^{\dagger\alpha 2}\frac{k'_\mu k_\alpha + k_\mu k'_\alpha}{k\cdot k'} \\ &\stackrel{3.31,3.32}{=} |M_{gg}^{11}|^2 + |M_{gg}^{22}|^2\end{aligned} \tag{3.36}$$

The terms including the unphysical polarization yield zero since k and k' are oriented along the z-direction. Thus, only the probabilities for producing transverse states $|M_{gg}^{11}|^2$ and $|M_{gg}^{22}|^2$ remain in eq. (3.36). So, the correct transition probability can be obtained by inserting the full polarization sum

$$\sum_{\lambda=1,2} \epsilon_\mu^{(\lambda)*}(k)\epsilon_\nu^{(\lambda)}(k) \rightarrow -g_{\mu\nu} + \frac{k^\nu k'^\mu + k^\mu k'^\nu}{k\cdot k'} \tag{3.37}$$

for one external gluon and eq. (3.33) for the other one. The last but least rigorous workaround is to assume that the gluons are transverse which should come out of the calculation instead of having to be put in. Nevertheless, this allows to simplify the third amplitude by employing the properties $\epsilon^{(\lambda)}(k)\cdot k = 0$ and $\epsilon^{(\lambda')}(k')\cdot k' = 0$, what results in

$$-i\widetilde{\mathfrak{M}}_3 = \frac{g_s^2}{s}(T_c)_{ij}f_{abc}\overline{u}(p',s')\left(2\gamma^\nu k^\mu + g^{\nu\mu}(\not{k'} - \not{k}) - 2\gamma^\mu k'^\nu\right)v(p,s)\epsilon_\nu(k,\lambda)\epsilon_\mu(k',\lambda'). \tag{3.38}$$

The amplitude arrived at in this way satisfies the Ward identity which can be easily verified using the results from eq. (3.26). Hence, the application of eq. (3.33) is legitimate. The last approach of including the ghost contributions shall be presented here.

Evaluation of the Dirac traces

The Dirac traces after applying the completeness relation in eq. (3.33) yield

$$\overline{|\mathfrak{M}_1|^2} \propto \frac{1}{4}\mathrm{Tr}((p\!\!\!/' + m_t)\gamma^\mu(p\!\!\!/' - k\!\!\!/' + m_t)\gamma^\nu(p\!\!\!/ - m_t)\gamma_\nu(p\!\!\!/' - k\!\!\!/' + m_t)\gamma_\mu) \tag{3.39}$$

$$\overline{|\mathfrak{M}_2|^2} \propto \frac{1}{4}\mathrm{Tr}((p\!\!\!/' + m_t)\gamma^\nu(k\!\!\!/' - p\!\!\!/ + m_t)\gamma^\mu(p\!\!\!/ - m_t)\gamma_\mu(k\!\!\!/' - p\!\!\!/ + m_t)\gamma_\nu) \tag{3.40}$$

$$\overline{|\mathfrak{M}_3|^2} \propto \frac{1}{4}\mathrm{Tr}((p\!\!\!/' + m_t)\gamma^\sigma(p\!\!\!/ - m_t)\gamma_\delta)\mathcal{M}^{\nu\mu}{}_\sigma\mathcal{M}_{\nu\mu}{}^\delta \tag{3.41}$$

$$\overline{\mathfrak{M}_1\mathfrak{M}_2^\dagger} \propto \frac{1}{4}\mathrm{Tr}((p\!\!\!/' + m_t)\gamma^\mu(p\!\!\!/' - k\!\!\!/' + m_t)\gamma^\nu(p\!\!\!/ - m_t)\gamma_\mu(k\!\!\!/' - p\!\!\!/ + m_t)) \tag{3.42}$$

$$\overline{\mathfrak{M}_1\mathfrak{M}_3^\dagger} \propto \frac{1}{4}\mathrm{Tr}((p\!\!\!/' + m_t)\gamma^\mu(p\!\!\!/' - k\!\!\!/' + m_t)\gamma^\nu(p\!\!\!/ - m_t)\gamma_\delta)\mathcal{M}_{\nu\mu}{}^\delta \tag{3.43}$$

$$\overline{\mathfrak{M}_2\mathfrak{M}_3^\dagger} \propto \frac{1}{4}\mathrm{Tr}((p\!\!\!/' + m_t)\gamma^\nu(k\!\!\!/' - p\!\!\!/ + m_t)\gamma^\mu(p\!\!\!/ - m_t)\gamma_\delta)\mathcal{M}_{\nu\mu}{}^\delta \tag{3.44}$$

$$\overline{|\mathfrak{M}_{\mathrm{ghost},1}|^2} \propto \frac{1}{4}\mathrm{Tr}((p\!\!\!/' + m_t)k\!\!\!/(p\!\!\!/ - m_t)k\!\!\!/) \tag{3.45}$$

$$\overline{|\mathfrak{M}_{\mathrm{ghost},2}|^2} \propto \frac{1}{4}\mathrm{Tr}((p\!\!\!/' + m_t)k\!\!\!/'(p\!\!\!/ - m_t)k\!\!\!/'). \tag{3.46}$$

The ghost expressions are multiplied with $\frac{1}{4}$ even though the initial ghost particles are excitations of a scalar field. This is due to the fact that these particles have the wrong relation between spin and statistics. These traces can be evaluated by means of the trace theorems given in [6, section 6.4], [11, appendix A.3] or [12, appendix A.4]. This is a straightforward but tedious calculation and that's why the TRACER [8] package for MATHEMATICA is used for the evaluation of these traces. The final results can be expressed again in terms of the Lorentz invariant Mandelstam variables (cf. eq. (3.3)).

$$\overline{|\mathfrak{M}_1|^2} = -\frac{2g_s^4 T_R^2\left(m_t^4 + m_t^2(3t + u) - tu\right)}{N\left(t - m_t^2\right)^2} \tag{3.47}$$

$$\overline{|\mathfrak{M}_2|^2} = -\frac{2g_s^4 T_R^2\left(m_t^4 + m_t^2(t + 3u) - tu\right)}{N\left(u - m_t^2\right)^2} \tag{3.48}$$

$$\overline{|\mathfrak{M}_3|^2} = -\frac{C_A g_s^4 T_R\left(27m_t^4 - 19m_t^2(t + u) + 4t^2 + 3tu + 4u^2\right)}{(N^2 - 1)\, s^2} \tag{3.49}$$

$$\overline{\mathfrak{M}_1\mathfrak{M}_2^\dagger} = \frac{2g_s^4 m_t^2 T_R^2\left(2m_t^2 + t + u\right)}{N\left(N^2 - 1\right)\left(t - m_t^2\right)\left(u - m_t^2\right)} \tag{3.50}$$

$$\overline{\mathfrak{M}_1\mathfrak{M}_3^\dagger} = -\frac{C_A g_s^4 T_R\left(3m_t^4 - m_t^2(3t + u) + t^2\right)}{(N^2 - 1)\, s\left(t - m_t^2\right)} \tag{3.51}$$

$$\overline{\mathfrak{M}_2 \mathfrak{M}_3^\dagger} = -\frac{C_A g_s^4 T_R \left(3 m_t^4 - m_t^2 (t + 3u) + u^2\right)}{\left(N^2 - 1\right) s \left(u - m_t^2\right)} \tag{3.52}$$

$$\overline{|\mathfrak{M}_{\text{ghost},1}|^2} = \overline{|\mathfrak{M}_{\text{ghost},2}|^2} = \frac{C_A g_s^4 T_R \left(m_t^2 - t\right)\left(m_t^2 - u\right)}{2\left(N^2 - 1\right) s^2} \tag{3.53}$$

3.4 The partonic cross section

Basically, the cross section σ is a measure of the probability that a scattering process takes place whereas the differential cross section $\frac{d\sigma}{d\Omega}$ contains information on the angular distribution. The cross section for a general collinear collision $A + B \rightarrow C + D$ is related to the invariant amplitude via the formula[3] [6, p. 90,91]

$$\begin{aligned}
d\sigma &= \frac{|\mathfrak{M}|^2}{F} d\Pi_{\text{Lips}} \\
&= \frac{|\mathfrak{M}|^2}{4\sqrt{(p_A \cdot p_B)^2 - m_A^2 m_B^2}} (2\pi)^4 \, \delta^{(4)}(p_C + p_D - p_A - p_B) \frac{d^3 p_C}{(2\pi)^3 2 E_C} \frac{d^3 p_D}{(2\pi)^3 2 E_D}
\end{aligned} \tag{3.54}$$

where the flux F ensures that the cross section is independent of the normalization of the incoming and outgoing states. For the collider setup defined in section 3.1, the above eq. (3.54) evaluates to

$$\frac{d\hat{\sigma}}{d\Omega} = \frac{\overline{|\mathfrak{M}|^2} \sqrt{1 - \frac{4 m_t^2}{\hat{s}}}}{64 \pi^2 \hat{s}}. \tag{3.55}$$

The hat indicates the separation between partonic and hadronic variables. So far, the invariant amplitude still depends on the kinetic invariants s, t and u. However, since the goal is to express the differential cross section in terms of measurable quantities s and θ the Mandelstam variables $v_+ \coloneqq t$ and $v_- \coloneqq u$ are replaced by (see eq. (3.1))

$$v_\pm = -\frac{\hat{s}}{2} + m_t^2 \pm \cos(\theta)\sqrt{\hat{s}\left(\frac{\hat{s}}{4} - m_t^2\right)}. \tag{3.56}$$

After putting $N = C_A = 3$, $T_R = \frac{1}{2}$ and $C_F = \frac{4}{3}$ as well as defining the strong coupling constant $\alpha_s \coloneqq \frac{g_s^2}{4\pi}$ the differential cross sections for top quark pair-production at lowest order can be determined to be

$$\frac{d\hat{\sigma}_{q\bar{q}}}{d\Omega} = \frac{\alpha_s^2 \beta \left(\cos^2(\theta)\beta^2 + \rho + 1\right)}{18 \hat{s}} \tag{3.57}$$

$$\begin{aligned}
\frac{d\hat{\sigma}_{gg}}{d\Omega} = \frac{\alpha_s^2 \beta}{192 \hat{s}\left(1 - \cos^2(\theta)\beta^2\right)^2} \Big(&-9 \cos^6(\theta)\beta^6 - \cos^4(\theta)\beta^4 \left(18\rho + 7\right) \\
&+ 7\left(-2\rho^2 + 2\rho + 1\right) + \cos^2(\theta)\left(18\rho^3 - 22\rho^2 - 5\rho + 9\right)\Big)
\end{aligned} \tag{3.58}$$

---

[3]The δ function was derived in eq. (2.31).

with $\rho = \frac{4m_t^2}{\hat{s}}$ and $\beta = \sqrt{1-\rho}$. After carrying out the integration over θ using MATHEMATICA, the total partonic cross sections yield

$$\hat{\sigma}_{q\bar{q}} = \frac{4\pi\alpha_s^2\beta\,(\rho+2)}{27\hat{s}} \tag{3.59}$$

$$\hat{\sigma}_{gg} = \frac{\pi\alpha_s^2\left(\left(2\rho^2+32\rho+32\right)\operatorname{artanh}\left(\beta\right)-\beta\left(31\rho+28\right)\right)}{48\hat{s}}. \tag{3.60}$$

These results are identical to the ones given in [9, p. 6].

3.5 The hadronic cross section

The calculated cross sections up to now are only valid for processes where quarks and gluons are brought to collision. However, as already mentioned, in pp and $p\bar{p}$ collisions the interactions take place between their constituents. These are the three valence quarks along with the so-called sea quarks (quark-antiquark pairs created due to the strong interaction) and gluons. As a consequence, the center-of mass-energy of the partonic collisions $\sqrt{\hat{s}}$ is not fixed even though the collision energy of the hadrons $\sqrt{S}$ is known. This issue is addressed by expressing $\hat{s}$ in terms of momentum fractions x_a ($0 \leq x_a \leq 1$) and x_b carried by the colliding partons a and b as follows:

$$\hat{s} = x_a x_b S. \tag{3.61}$$

The momentum density of partons a within a proton is encoded in the parton distribution function $f_a(x, \mu_F)$. The latest "measurement" by the CTEQ collaboration is shown in fig. 3.2. The factorization scale μ_F is a measure to separate low energy "soft" physics describing bound states from high energy "hard" processes. Then, the hadronic cross section σ can be obtained by integrating over all possible energies and momentum fractions [10, p. 14]

$$\begin{aligned}
\frac{d\sigma}{d\cos\theta} &= \sum_{a,b}\int_{\hat{s}_{\min}}^{S}d\hat{s}\int_{\frac{\hat{s}}{S}}^{1}dx_1\int_{\frac{\hat{s}_{\min}}{Sx_1}}^{1}dx_2\delta(\hat{s}-x_1x_2S)f_a(x_1,\mu_F)f_b(x_2,\mu_F)\frac{d\hat{\sigma}_{ab}}{d\cos\theta} \\
&= \sum_{a,b}\int_{\hat{s}_{\min}}^{S}d\hat{s}\int_{\frac{\hat{s}}{S}}^{1}dx_1\frac{1}{x_1S}f_a(x_1,\mu_F)f_b\left(\frac{\hat{s}}{x_1S},\mu_F\right)\frac{d\hat{\sigma}_{ab}}{d\cos\theta}.
\end{aligned} \tag{3.62}$$

The integration limits arise from the inequality $\frac{\hat{s}}{S} \leq x_1x_2 \leq 1$. The integration variable x_2 is eliminated by evaluating the Dirac delta function

$$\delta(\hat{s}-x_1x_2S) = \delta\left(x_1S\left(\frac{\hat{s}}{x_1S}-x_2\right)\right) = \frac{1}{x_1S}\delta\left(\frac{\hat{s}}{x_1S}-x_2\right). \tag{3.63}$$

The minimal partonic c.m. energy $\hat{s}_{\min}$ is defined trough the partonic cross sections themselves since these take complex values for $\hat{s}_{\min} := 4m_t^2 \geq \hat{s}$. The difference between a proton-proton collider and an antiproton-proton collider is hidden in the sum. Since the parton distribution functions for antiquarks and quarks in a proton differ from each other, both possibilities, that quark a comes from proton 1 and quark b from proton 2 and vice versa, must be included. However, the PDF for an antiquark in an antiproton is identical to the PDF for a quark in a proton, which is why there is only one possibility for the $p\bar{p}$ collider. So far, the cross section is still given in natural units. To obtain the SI unit m^2 the result has to be multiplied with $\hbar^2 c^2$. Usually, cross sections are given in the unit barn $1\,\mathrm{b} = 10^{-28}\,\mathrm{m}^2$.
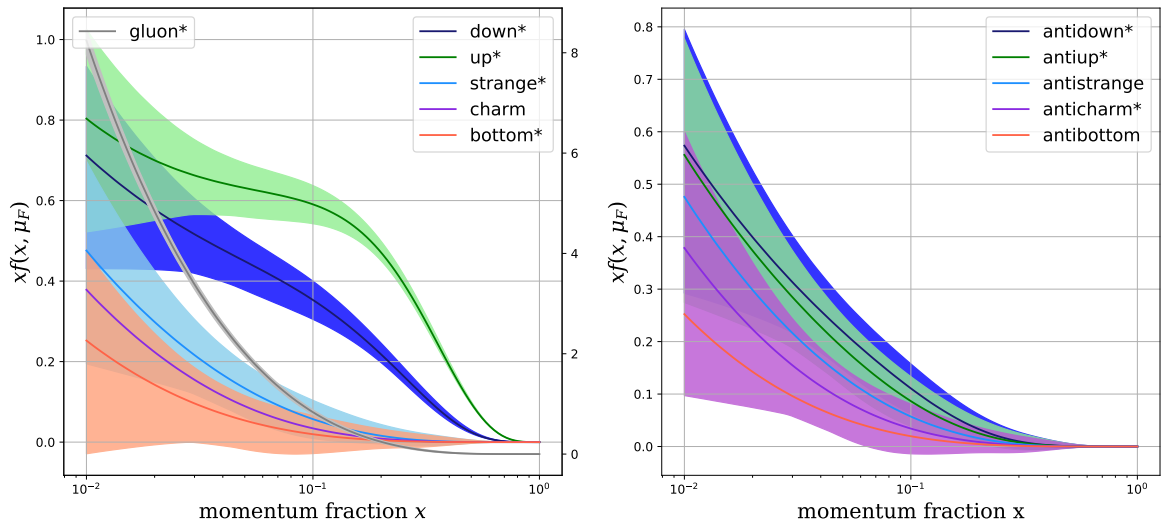

Figure 3.2: Illustration of the parton distribution functions $f_a(x, \mu_F)$ at a scale $\mu_F = 173.3\,\mathrm{GeV}$ (the top quark mass) based on the PDF set CT14nlo [5] and created with LHAPDF 6 [1]. The PDFs for those partons marked with an asterisk are shown along with their uncertainties. For reasons of clarity, the gluon distribution is plotted on a second axis.

4 Numerical analysis and results

The integral for the hadronic cross section developed in the previous chapter is computed using Monte Carlo integration, an integration technique based on random numbers. The probabilistic nature of this method allows the simulation of events which is performed within the Hit-or-Miss Monte Carlo approach. The associated code is written in PYTHON 3. The strong coupling constant $\alpha_s(\mu_R)$, illustrated in fig. 2.1b, as well as the parton distribution functions shown in fig. 3.2 are determined via the PYTHON 3 interface for LHAPDF 6 [1] based on the PDF set CT14nlo [5]. To demonstrate the explicit procedure and numerical methods the code is embedded at appropriate points. To understand the code pieces it is necessary to know the used PYTHON 3 modules and global variables.

```python
#use "export python=/path/to/python3" in order to install LHAPDF
#for python 3 before running "configure.sh"
import lhapdf
import matplotlib.pyplot as plt
import numpy as np
import random
import sys
import matplotlib as mpl
from mpl_toolkits.mplot3d import Axes3D

#seed for random numbers
seed = 12342
random.seed(seed)

#initialize PDF member object (for protons) and load whole set
p = lhapdf.mkPDF("CT14nlo",0)
pdf_set = p.set()
pdf_members = pdf_set.mkPDFs()

#conversion between natural and SI units (taken from particle data group)
CONVERSION_CONSTANT = 0.38937936561e9 #GeV^2 picobarn
```

```python
def update(counter, max_counter):
    if((counter*100.)/max_counter)%10 == 0:
        sys.stdout.write(str(int((counter*100.)/max_counter))+"% ")
        sys.stdout.flush()
```

4.1 Monte Carlo integration

The integral for the hadronic cross section in eq. (3.62) is evaluated numerically using the
Monte Carlo method. The basic idea behind this procedure is to approximate an integral
of a function $f : \mathbb{R}^n \to \mathbb{R}$ by averaging over the integrand where the supporting points
$x_1, ..., x_N \in \Omega \subseteq \mathbb{R}^n$ are generated randomly

$$I = \int_\Omega f d\mu = \mu(\Omega)\langle f \rangle \approx \mu(\Omega)\frac{1}{N}\sum_{i=1}^N f(x_i). \tag{4.1}$$

According to the central limit theorem the distribution $\langle f \rangle$ will tend to a Gaussian for great
N with the standard deviation

$$\sigma_{\mathrm{MC}} = \frac{\sigma}{\sqrt{N}} \tag{4.2}$$

where

$$\sigma^2 = \sum_{i=1}^N \left(\langle f \rangle - f(x_i)\right)^2 = \langle f \rangle^2 - \langle f^2 \rangle \tag{4.3}$$

is the variance of f. This gives an estimate of the accuracy. In addition, Monte Carlo inte-
gration is capable of computing integrals in which the integration limits are interdependent
as outlined in [7, chapter 6]. If one considers a triangular integration region, as is the case in
eq. (3.62), picking $\hat{s}$ at first and afterwards a value for x_1 between $\frac{\hat{s}}{S}$ and 1 leads to a much
higher density of points in the area for great $\hat{s}$. To avoid this problem, two random values r_1
and r_2 are generated (equivalent to choosing points over the square to ensure a homogeneous
density) and then assigned to the integration variables in the following way:

$$s = \min(r_1, r_2)(S - 4m_t^2) + 4m_t^2$$
$$x_1 = \max(r_1, r_2)(1 - \frac{\hat{s}}{S}) + \frac{4m_t^2}{S}. \tag{4.4}$$

Choosing the minimal and maximal value guarantees that all points fall into the triangle.
The only thing missing is the integration region which is given by

$$\int_{4m_t^2}^S d\hat{s} \int_{\hat{s}/S}^1 dx_1 = \frac{8m_t^4}{S} - 4m_t^2 + \frac{S}{2}. \tag{4.5}$$

So, a basic random value generator for the integral in eq. (3.62) can be implemented as
follows:

```python
class simple_random_value_generator():
    def __init__(self,m_top,cms_energy):
        self.S = cms_energy**2
        self.s0 = 4*m_top**2


    def generate_random_values(self):
        r1 = random.random()
        r2 = random.random()


        s = min(r1,r2)*(self.S-self.s0)+self.s0
        x1 = max(r1,r2)*(1-self.s0/self.S)+self.s0/self.S
        cos = random.random()*2-1


        x2 = s/(x1*self.S)
        jacobian = 1
        return (cos,s,x1,x2,jacobian)

    def integration_area(self):
        return -self.s0+self.s0**2/(2*self.S)+self.S/2
```

4.2 Importance Sampling

Looking at eq. (4.2), the Monte Carlo error can be reduced by increasing the number of
samples or by decreasing the variance of f. In order to save run time, the second option
appears as the more attractive solution. Variance reduction can be achieved by a method
called "importance sampling". In the ideal case, this means finding a function y whose
Jacobian determinant cancels the integrand

$$f(y(x)) \left| \det Dy(x) \right| = 1 \tag{4.6}$$

which is more obvious in the one dimensional case. Let the new integration variable y be the
integral of $f(x) \geq 0 \; \forall x \; \in \Omega$

$$y(x) = \int f(x) \; dx, \tag{4.7}$$

so that the integrand yields one after applying the inverse function theorem

$$f(x)dx = f(x(y)) \left| \frac{\partial x(y)}{\partial y} \right| dy = f(y) \left| \frac{1}{\frac{\partial y}{\partial x}(y)} \right| dy = f(y) \frac{1}{f(y)} \, dy = dy.$$

However, if this were possible, there would be no need for any numerical integration. For this reason, the goal is to find a function that approximates the integrand and owns an invertible antiderivative. The second requirement is already fulfilled by the assumption $f \geq 0$. By
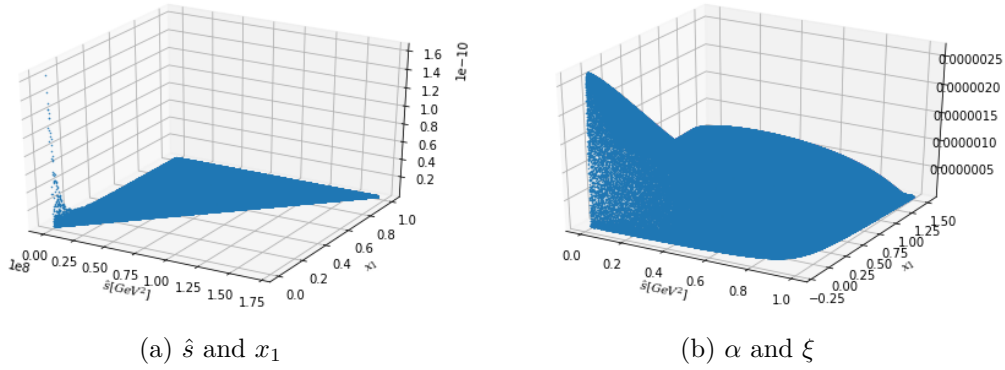

(a) $\hat{s}$ and x_1 (b) α and ξ

Figure 4.1: Plots of the integrand in eq. (3.62) in the "natural" variables $\hat{s}$ and x_1 as well as the new ones α and ξ (for $a = 0.1$ and $b = 0.5$) for the LHC collider with the parameters $m_t = 173.3$ GeV, $\mu_R = \mu_F = m_t$ and $S = 13$ TeV.

looking at cross sections of the integrand in fig. 4.1a the two approximations

$$h(\hat{s}) = \frac{\sqrt{\hat{s} - 4m_t^2}}{\hat{s}^{\frac{5}{2}}} \tag{4.8}$$

$$g(x_1) = \frac{1}{(x_1 - a^2)^2 + a^2 b^2} \tag{4.9}$$

seem reasonable where the constants $a = 0.1$ and $b = 0.5$ are left to be determined for other choices of the integration parameters than the ones given in fig. 4.1. However, testing different parameters has shown that these values generally lead to good results[1]. After integration one obtains the new variables

$$\xi(\hat{s}) = \left(\frac{\hat{s} - 4m_t^2}{\hat{s}} \right)^{\frac{3}{2}} \tag{4.10}$$

$$\alpha(x_1) = \arctan\left(\frac{x_1 - a^2}{ab} \right) \tag{4.11}$$

---

[1]E.g. the "natural" variables $\hat{s}$ and x_1 lead to a success rate of $\sim 0.008\,\%$ in terms of event generation whereas the new ones ξ and α achieved $\sim 31\,\%$ for the parameters given in fig. 4.1

where every proportional factor was omitted since these cancel those factors occurring during the random value generation. The Jacobian can be determined to be

$$\frac{\partial \hat{s}}{\partial \xi}\frac{\partial x_1}{\partial \alpha} = \frac{8m_t^2}{(3\xi^{\frac{1}{3}}(1-\xi^{\frac{2}{3}})^2)}\frac{ab}{\cos\alpha^2}. \tag{4.12}$$

The integration region is given by

$$\int_0^{\xi_{\max}} d\xi \int_{\alpha_{\min}}^{\alpha_{\max}} d\alpha = \int_{4m_t^2}^S d\hat{s} \int_{\frac{\hat{s}}{S}}^1 dx_1 \frac{\sqrt{\hat{s}-4m_t^2}}{\hat{s}^2}\arctan\left(\frac{\frac{\hat{s}}{S}-a^2}{ab}\right) = \alpha_{\max}\xi_{\max}-I \quad (4.13)$$

with the new limits of integration $\alpha_{\max}=\alpha(1)$, $\alpha_{\min}=\alpha\left(\frac{\hat{s}}{S}\right)$ and $\xi_{\max}=\xi(S)$ where the integral I is evaluated by means of MATHEMATICA

$$\begin{aligned}
I =&6m_t^2 \int_{4m_t^2}^S d\hat{s}\frac{\sqrt{\hat{s}-4m_t^2}}{\hat{s}^2}\arctan\left(\frac{\frac{\hat{s}}{S}-a^2}{ab}\right) = \frac{2}{2a^2S^2\left(a^2+b^2\right)^{3/2}}\\
&\times\left(\frac{a^2}{S}\arctan\left(\frac{1-a^2}{ab}\right)\left(S\left(a^2+b^2\right)\left(S-4m_t^2\right)\right)^{3/2}\right.\\
&+(a-ib)^{3/2}\left(-ia^2S+abS+i4m_t^2\right)\\
&\times\sqrt{aS\left(-a^2S-iabS+4m_t^2\right)}\arctan\left(\frac{\sqrt{a(a+ib)(S-4m_t^2)}}{\sqrt{-a^2S-iabS+4m_t^2}}\right)\\
&+\sqrt{aS(a+ib)}\left((a+ib)\left(ia^2S+abS-i4m_t^2\right)\sqrt{-a^2S+iabS+4m_t^2}\right.\\
&\left.\left.\times\arctan\left(\frac{\sqrt{a(a-ib)(S-4m_t^2)}}{\sqrt{-a^2S+iabS+4m_t^2}}\right)-8bm_t^2\sqrt{a(a-ib)(S-4m_t^2)}\right)\right).
\end{aligned} \tag{4.14}$$

The result for I contains the sum of a complex number with its complex conjugate which ensures a real valued and simplified expression[2]:

$$\begin{aligned}
I =&\frac{2}{2a^2S^2\left(a^2+b^2\right)^{3/2}}\left(-8abm_t^2\sqrt{S\left(a^2+b^2\right)\left(S-4m_t^2\right)}\right.\\
&+\frac{a^2}{S}\arctan\left(\frac{1-a^2}{ab}\right)\left(S\left(a^2+b^2\right)\left(S-4m_t^2\right)\right)^{3/2}\\
&+2\operatorname{Re}\left(\left(a-ib\right)^{3/2}\left(-ia^2S+abS+i4m_t^2\right)\sqrt{aS\left(-a^2S-iabS+4m_t^2\right)}\right.\\
&\left.\left.\times\arctan\left(\frac{\sqrt{a(a+ib)(S-4m_t^2)}}{\sqrt{-a^2S-iabS+4m_t^2}}\right)\right)\right).
\end{aligned} \tag{4.15}$$

---

[2]The complex conjugate of a square root can be obtained in the following way. Let be $y=z^2$, where $y,z\in\mathbb{C}$. Hence, the square root is given by $z=\sqrt{y}$. Taking the complex conjugate of z^2 yields $\left(z^2\right)^*=z^*z^*=y^*$ which means $z^*=\sqrt{y^*}$. The identity $\arctan(z)^*=\arctan(z^*)$ results directly from the series representation.

The issue of interdependent integration limits cannot be solved in the same manner as before since the integration region does not correspond to a triangle anymore. Therefore, ξ and α are generated over the whole square but those values for α smaller than $\alpha_{\min}$ are rejected. However, since the integration area corresponds nearly to a square, as shown in fig. 4.1b, the rejection rate is less than 1%. The new value generator containing importance sampling is implemented in the following way:

```python
class random_value_generator_importance_sampling():
    def __init__(self,m_top,cms_energy,a,b):
        self.S = cms_energy**2
        self.s0 = 4*m_top**2
        self.a = a
        self.b = b


        #definition of values that are constant throughout
        #the value generation process
        self.xi_max = (1-4*m_top**2/cms_energy**2)**(3./2)
        self.lowest_alpha = np.arctan((4*m_top**2/cms_energy**2-a**2)/(a*b))
        self.alpha_max = np.arctan((1-a**2)/(a*b))


    def generate_random_values(self):
        #kind of an emulation of a do-while loop
        alpha = 0
        alpha_min = 1


        #search for alpha and xi that are within the integration region
        while alpha < alpha_min:
            #generate xi
            xi = random.random()*self.xi_max
            s = self.s0/(1-(xi)**(2./3))
            alpha_min = np.arctan((s/self.S-self.a**2)/(self.a*self.b))
            #generate alpha
            r = random.random()
            alpha = r*self.alpha_max+self.lowest_alpha*(1-r)


        #calculate x1 and x2 through generated alpha and s
        x1 = (self.a*self.b*np.tan(alpha)+self.a**2)
```

```python
        x2 = s/(x1*self.S)


        #generate cos
        cos = random.random()*2-1


        #caluclate jacobian
        jacobian = 2*self.s0/(3*xi**(1./3)*(1-xi**(2./3))**2)   #s --> xi
        jacobian *= self.a*self.b/(np.cos(alpha)**2) #x1 --> alpha


        return (cos,s,x1,x2,jacobian)


    def integration_area(self):
        return self.alpha_max*self.xi_max-self.I()


    def I(self):
        return  (...)
```

4.3 Computation of the hadronic cross section

The hadronic cross section along with its numerical uncertainty is calculated using the Monte Carlo method described above. Usually, a PDF set contains a "central" set along with a number of other sets (CT14nlo consists of 57 members in total) allowing to give an estimate on the PDF uncertainty. To account for the uncertainty due to higher order corrections the renormalization and factorization scales are varied.

4.3.1 Implementation of the Monte Carlo procedure

In order to enable the computation of total cross sections, the implementation of the corresponding mathematical expressions is necessary at first.

```python
def rho_and_beta(s,m_top):
    rho = 4*m_top**2/s
    beta = np.sqrt(1-rho)
    return (rho,beta)


def total_cross_section_qqbar(s,m_top,alpha_s):
    rho,beta = rho_and_beta(s,m_top)
    return (...)
```

```python
def total_cross_section_gg(s,m_top,alpha_s):
    rho,beta = rho_and_beta(s,m_top)
    return (...)


def integrand_gg(pdf_member,S,x1,x2,mu_f,cross_sec_func,cross_sec_args):
    pdf_value = pdf_member.xfxQ(21,x1,mu_f)*pdf_member.xfxQ(21,x2,mu_f)
    return pdf_value*cross_sec_func(*cross_sec_args)/(x1**2*x2*S)


def integrand_qqbar(pdf_member,S,x1,x2,mu_f,cross_sec_func,
                cross_sec_args,collider):
    integrand_qqbar = 0
    for flavour in range(1,6):
        pdf_value = (pdf_member.xfxQ(flavour,x1,mu_f)*
                    pdf_member.xfxQ(collider*flavour,x2,mu_f))
        if collider == -1:
            pdf_value += (pdf_member.xfxQ(flavour,x2,mu_f)*
                        pdf_member.xfxQ(-flavour,x1,mu_f))
        integrand_qqbar += (pdf_value*cross_sec_func(*cross_sec_args)/
                        (x1**2*x2*S))
    return integrand_qqbar
```

The functions `integrand_gg` and `integrand_qqbar` are designed in such a way that they work for any cross section passed within the parameter `cross_sec_func` along with its arguments `cross_sec_args`. The parameter `collider` takes the value -1 for a pp and 1 for a $p\bar{p}$ collider. The hadronic cross section can then be computed using this function:

```python
def hadronic_cross_section(pdf_member,cm_energy,N,
                            collider,m_top,mu_f,mu_r,value_generator):
    #mu_f and mu_r are supposed to have the unit GeV
    S = cm_energy**2
    alpha_s = pdf_member.alphasQ(mu_r)

    #contains sigma_qqbar, sigma_gg, sigma_total as well as
    #Monte Carlo error/squared values of the integrand
    sigma = np.array([[0.,0.]]*3)

    #generation of N_supporting_points in phase space
```

```python
for i in range(N):
    #show progress
    update(i, N)


    #generation of values
    cos,s,x1,x2,jacobian = value_generator.generate_random_values()
    cross_sec_args = [s,m_top,alpha_s]


    #calculation of weights for both partonic channels
    w_gg = integrand_gg(pdf_member,S,x1,x2,mu_f,
                        total_cross_section_gg,cross_sec_args)
    w_qqbar = integrand_qqbar(pdf_member,S,x1,x2,mu_f,
                              total_cross_section_qqbar,
                              cross_sec_args,collider)
    w = np.array([w_gg,w_qqbar,w_gg+w_qqbar])
    w *= jacobian


    #adding weights to total cross section
    sigma[:,0] += w
    sigma[:,1] += w**2


#integration area is dependent on choice of integration variables
integration_area = value_generator.integration_area()

#multiply by integration area, average and transform to picobarn
sigma *= integration_area/N
sigma[:,0] *= CONVERSION_CONSTANT
sigma[:,1] *= CONVERSION_CONSTANT**2


#calculation of Monte Carlo errors
sigma[:,1] = np.sqrt(np.absolute(sigma[:,1]-sigma[:,0]**2)/N)


#returns cross sections as well as Monte Carlo errors
return sigma
```

4.3.2 PDF uncertainties

The PDF uncertainties are computed following the prescriptions given in [2, p. 4]. Since both, the strong coupling constant and the parton distribution function, are generated on the basis of the PDF set, this definition is extended to both quantities. For the CTEQ family of sets the uncertainty is typically given in the form of an asymmetric error

$$\Delta\sigma_{\mathrm{PDF}+\alpha_s}^+ = \sqrt{\sum_i \left(\max\left(\sigma(set_{+i}) - \sigma(set_0), \sigma(set_{-i}) - \sigma(set_0), 0\right)\right)^2} \qquad (4.16)$$

$$\Delta\sigma_{\mathrm{PDF}+\alpha_s}^- = \sqrt{\sum_i \left(\max\left(\sigma(set_0) - \sigma(set_{+i}), \sigma(set_0) - \sigma(set_{-i}), 0\right)\right)^2} \qquad (4.17)$$

where all cross sections are evaluated with the "central" scale choices $\mu_F = m_t$ and $\mu_R = m_t$. The sum in eq. (4.17) runs over all pairs of PDFs in the given set. The central set is denoted by $\sigma(set_0)$. All odd pairs are represented by $\sigma(set_{+i})$ and the even ones by $\sigma(set_{-i})$. The PDF errors exceed the numerical ones by at least one order of magnitude, which is why the latter is not taken into account.

```python
def cross_section_pdf_alphas_error(cm_energy,N_supporting_points,
                                   collider,m_top,value_generator):
    #sigmas contains cross sections (qqbar, gg and total) for every member
    sigmas = []
    for pdf_member in pdf_members:
        #all cross sections are evaluated at mu_r = mu_f = m_top
        sigma = hadronic_cross_section(pdf_member,cm_energy,
                                       N_supporting_points,collider,m_top,
                                       m_top,m_top,value_generator)
        sigmas.append(sigma[:,0])


    #calculation of asymmetric errors
    error_plus,error_minus,zero_array = (np.zeros(3),np.zeros(3),np.zeros(3))
    central = sigmas[0]
    for i in range(1,int((len(sigmas)+1)/2)):
        odd  = sigmas[2*i-1] - central;
        even = sigmas[2*i] - central;
        #determine max
        error_plus += np.amax([even,odd,zero_array],axis=0)**2
        error_minus += np.amax([-even,-odd,zero_array],axis=0)**2
```

```python
    error_plus = np.sqrt(error_plus)
    error_minus = np.sqrt(error_minus)


    #output errors in the shape [[qqbar +,-], [gg +,-], [total +,-]]
    return np.column_stack((error_plus,error_minus))
```

4.3.3 Scale variation

Ideally, when calculating the hadronic cross section up to all orders, the result is independent of the initial scale choices. However, at leading order the cross section depends heavily on the scales μ_F and μ_R. Therefore, the scales are varied around the top mass in the regions $\frac{1}{2} \leq \frac{\mu_F}{\mu_R} \leq 2$. The uncertainties are then computed by taking the minimal and maximal deviation from the "central" scales $\mu_F = m_t$ and $\mu_R = m_t$ as explained in [2, p. 3]:

$$\Delta\sigma_\mu^+ = \max_{\{\mu_R,\mu_F\}} \left(\sigma(\mu_F,\mu_R) - \sigma(m_t,m_t)\right) \tag{4.18}$$

$$\Delta\sigma_\mu^- = -\min_{\{\mu_R,\mu_F\}} \left(\sigma(\mu_F,\mu_R) - \sigma(m_t,m_t)\right). \tag{4.19}$$

In general, the results obtained by varying around the three values $0.5m_t$, m_t and $2m_t$ differ barely from a fine scan with more values. The corresponding implementation looks as follows.

```python
def cross_section_scale_error(cm_energy,N,collider,
                              m_top,mu_f_list,mu_r_list,value_generator):
    #both lists (mu_r_list and mu_f_list) are
    #assumed to be in units of the top quark mass
    sigmas = []
    counter, central_index = 0,0


    #mu_r = 1 and mu_f = 1 are supposed to be included in the lists
    for mu_r in mu_r_list:
        for mu_f in mu_f_list:
            if 0.5 <= mu_f/mu_r and mu_f/mu_r <= 2:
                #find central cross section
                if mu_f == 1 and mu_r == 1:
                    central_index = counter
                #all cross sections are evaluated with the central PDF set
                sigma = hadronic_cross_section(p,cm_energy,N,collider,
                                               m_top,mu_f*m_top,mu_r*m_top,
                                               value_generator)
```

```
                #save cross section and increment counter
                sigmas.append(sigma[:,0])
                counter += 1


        #calculate the error for the respective cross section
        sigma_central = sigmas[central_index]
        error_plus = np.amax(sigmas,axis=0)-sigma_central
        error_minus = sigma_central-np.amin(sigmas,axis=0)


        #output errors in the shape [[qqbar +,-], [gg +,-], [total +,-]]
        return np.column_stack((error_plus,error_minus))
```

4.3.4 Results

As depicted in detail above, Standard Model predictions for the hadronic cross section at tree level for $t\bar{t}$ production are obtained using Monte Carlo integration implemented in PYTHON 3 based on the partonic cross sections outlined in chapter 3. The number of supporting points is set to $N = 10\,000$ and the top quark mass is chosen to be $m_t = 173.3\,\mathrm{GeV}$ [3, p. 2]. The scales are varied around $\frac{m_t}{2}$, m_t and $2m_t$. The results for various accelerators and c.m. energies are presented in table 4.1 and confirmed by the program TOP++ [4].

Table 4.1: Leading order predictions for the total hadronic cross section in pb including uncertainties for various colliders and energies subdivided into the different partonic channels.

collider	channel	σ	Monte Carlo	PDF+α_s	scales
LHC 13 TeV	$gg \to t\bar{t}$	411.49	0.21(0.05 %)	+33.94(8.2 %) −14.39(3.5 %)	+126.63(30.8 %) −91.15 (22.2 %)
	$q\bar{q} \to t\bar{t}$	65.91	0.12(0.18 %)	+4.03(6.1 %) −1.53(2.3 %)	+14.99(22.7 %) −10.67 (16.2 %)
	$pp \to t\bar{t}$	477.40	0.27(0.06 %)	+35.62(7.5 %) −13.52(2.8 %)	+140.93(29.5 %) −101.81 (21.3 %)
LHC 7 TeV	$gg \to t\bar{t}$	78.862	0.023(0.03 %)	+7.22(9.1 %) −7.01(8.9 %)	+29.8(37.8 %) −19.87 (25.2 %)
	$q\bar{q} \to t\bar{t}$	23.597	0.022(0.09 %)	+0.99(4.2 %) −1.5(6.4 %)	+6.16(26.1 %) −4.5 (19.1 %)
	$pp \to t\bar{t}$	102.459	0.023 (0.02 %)	+7.04(6.9 %) −7.39(7.2 %)	+35.96(35.1 %) −24.37 (23.8 %)
Tevatron 1.96 TeV	$gg \to t\bar{t}$	0.4572	0.0027 (0.59 %)	+0.14(31.5 %) −0.13(28.8 %)	+0.26(57.5 %) −0.16 (35.7 %)
	$q\bar{q} \to t\bar{t}$	4.837	0.025 (0.51 %)	+0.06(1.3 %) −0.38(7.8 %)	+1.79(36.9 %) −1.28 (26.6 %)
	$p\bar{p} \to t\bar{t}$	5.294	0.027(0.52 %)	+0.08(1.6 %) −0.42(8.0 %)	+2.05(38.7 %) −1.45 (27.4 %)

It has been confirmed that the leading order results strongly depend on the choice of scales. E.g. the cross section for gg-fusion at LHC at $7\,\mathrm{TeV}$ may vary up to $37.8\,\%$ due to scale variation while the NNLO result including soft-gluon resummation at next-to-next-to-leading-log order calculated with the TOP++ program is $\left(148.103^{+17.6338(11.9064\,\%)}_{-17.5814(11.8711\,\%)}\,(\mathrm{scale})\,\right)$ pb. This result also demonstrates the necessity to resort to higher order perturbation theory in order to obtain experimentally comparable results. However, the results indicate that $q\bar{q}$-annihilation is with $92\,\%$ the dominant production channel at Tevatron whereas $86\,\%$ of the top pairs produced at the LHC at $\sqrt{S} = 13\,\mathrm{TeV}$ are due to gluon fusion which is confirmed experimentally [3, p. 2].

4.4 Hit-or-Miss event generation

Monte Carlo event generators have become an essential tool to bridge the gap between theoretical calculations and detector signals, thus allowing to make predictions for future experiments. The event generator created in this work is used to simulate the first stage of the structure of an event at the LHC - the hard process. The close relation between the Monte Carlo method and the physical process in being random is exploited for this purpose.

4.4.1 Method

Every phase space point generated during the integration process can be regarded as an event. The value of the integrand at the respective point, also called weight, corresponds to the probability of the event occurring. The storage of each event along with its weight is very inefficient that's why the Hit-or-Miss method is a suitable choice to unweight or equalize the events. Practically, this can be done by finding the maximum weight W_{max} and then comparing the probability $\frac{W_i}{W_{\mathrm{max}}}$ of each randomly generated point with weight W_i to a random number R. If $\frac{W_i}{W_{\mathrm{max}}} > R$ the event is accepted otherwise rejected. This process is repeated until the desired number of N_{events} generated events is reached. To obtain information on the angular distribution, the differential cross sections are used for the simulation.

```python
def diff_cross_section_qqbar(s,cos,m_top,alpha_s):
    rho,beta = rho_and_beta(s,m_top)
    return (...)


def diff_cross_section_gg(s,cos,m_top,alpha_s):
    rho,beta = rho_and_beta(s,m_top)
    return (...)
```

The event generation is then performed using this function:

```python
def generate_events(cms_energy,N_max,N_events,collider,
                    m_top,mu_f,mu_r,value_generator):
    S = cms_energy**2
    #the central PDF set is used for event generation
    alpha_s = p.alphasQ(mu_r)
    integrand_max = 0


    #find max
    sys.stdout.write("Find max: ")
    for i in range(N_max):
        #show progress
        update(i, N_max)
        #generation of values to find max of integrand within N_max tries
        cos,s,x1,x2,jacobian = value_generator.generate_random_values()
        cross_sec_args = [s,cos,m_top,alpha_s]
        integrand = integrand_gg(p,S,x1,x2,mu_f,
                                 diff_cross_section_gg,cross_sec_args)
        integrand += integrand_qqbar(p,S,x1,x2,mu_f,diff_cross_section_qqbar,
                                     cross_sec_args,collider)
        integrand *= jacobian
        if integrand_max < integrand:
            integrand_max = integrand


    #Hit-or-Miss Monte Carlo envent generation
    events = np.zeros((4,N_events)) # contains s, cos, x1, x2

    hit_counter = 0 #counts "real" events
    old_hit_counter = hit_counter #for update function
    event_counter = 0 #total number of generated events for success rate

    sys.stdout.write("\nEvent generation: ")
    while hit_counter < N_events:
        event_counter += 1
        #show progress
        if hit_counter > old_hit_counter:
            old_hit_counter =  hit_counter
```

```python
        update(hit_counter, N_events)


    #generate events and save hits
    cos,s,x1,x2,jacobian = value_generator.generate_random_values()
    cross_sec_args = [s,cos,m_top,alpha_s]
    integrand = integrand_gg(p,S,x1,x2,mu_f,
                             diff_cross_section_gg,cross_sec_args)
    integrand += integrand_qqbar(p,S,x1,x2,mu_f,
                                 diff_cross_section_qqbar,
                                 cross_sec_args,collider)
    integrand *= jacobian
    if integrand_max*random.random() < integrand:
        events[:,hit_counter] = s,cos,x1,x2
        hit_counter += 1


print("\nSuccess rate: "+str(N_events*100/event_counter)+"%")
return (events[0],events[1],events[2],events[3])
```

4.4.2 Results

The event generation is performed for Tevatron at $1.96\,\text{TeV}$ and for LHC at $13\,\text{TeV}$. For both cases $1\,000\,000$ events are simulated at the scales $\mu_R = m_t$ and $\mu_F = m_t$ where the top mass is chosen to be $173.3\,\text{GeV}$. As described in section 3.1 the momenta and energies of the top pair are measured in the lab frame. Since the transverse momentum is invariant under the Lorentz transformation given in eq. (3.2) where the velocity is given by $\beta = \frac{x_2-x_1}{x_1+x_2}$, no information is lost and it makes sense to split the momentum in the lab frame into a longitudinal and transverse part:

$$
\begin{aligned}
p_{\text{trans}} &= \sum_{a=t,\bar{t}} \sqrt{p_1^{\text{lab}}(a)^2 + p_2^{\text{lab}}(a)^2} \\
p_{\text{long}} &= \sum_{a=t,\bar{t}} \left| p_3^{\text{lab}}(a) \right| \\
p_{\text{lab}} &= \sqrt{p_{\text{trans}}^2 + p_{\text{long}}^2}.
\end{aligned}
\tag{4.20}
$$

The energy of the $t\bar{t}$-pairs in the center-of-mass frame as well as in the lab frame $E_{\text{lab}} = p_0^{\text{lab}}$ for both colliders are displayed as histograms in fig. 4.2. The peak in the c.m. system is just as easily visible in the laboratory system. The fact that the Tevatron probes significantly smaller energies than the LHC is also reflected in the number of events generated.
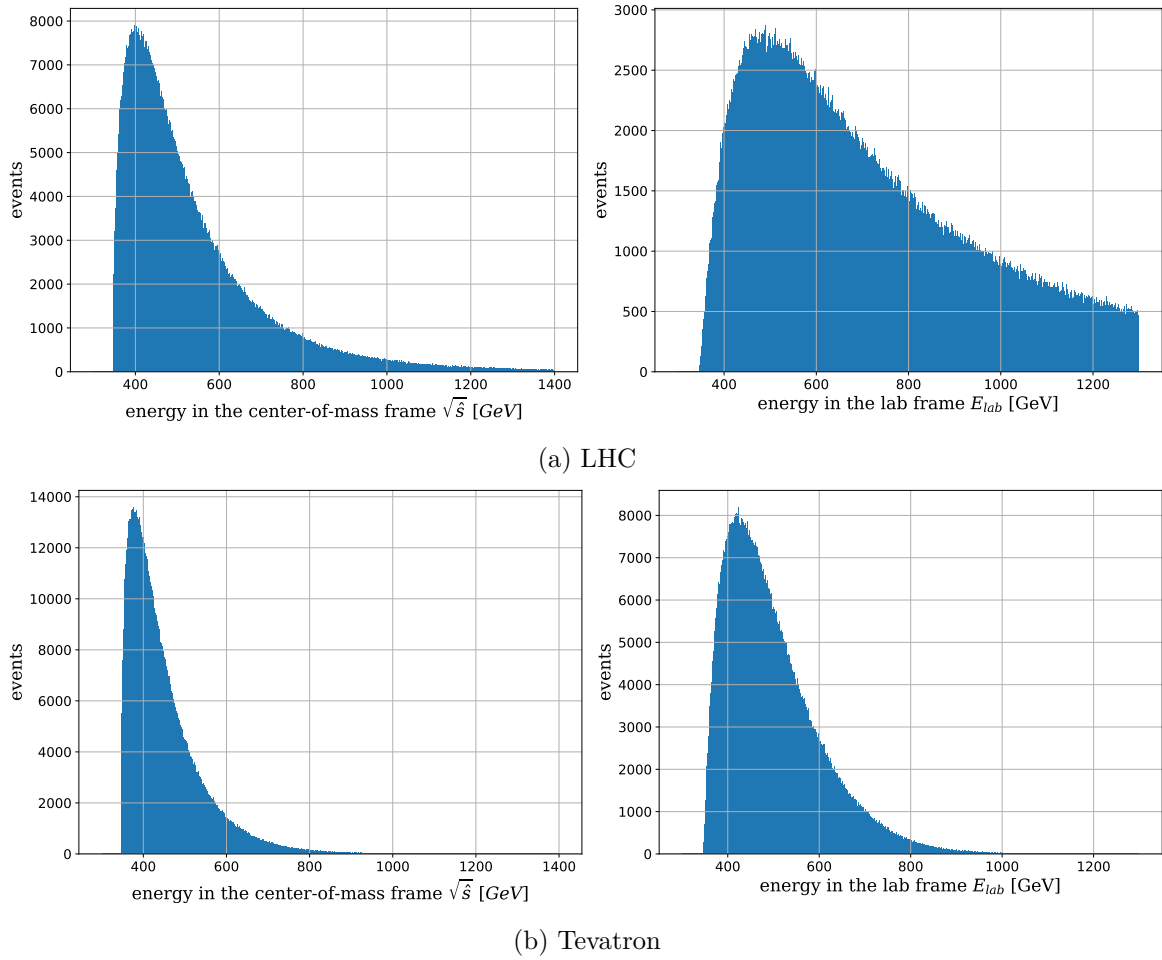
(a) LHC

(b) Tevatron

Figure 4.2: Energies of the generated events in the c.m.s. of the quarks and in the lab frame presented as histogram.

In the histograms presenting the momentum of the top quarks fig. 4.3 it can be seen that most events are not generated at the top quark mass ($p_{\text{lab}} = 0$), but at a higher energies $\sim 375\,\text{GeV}$ for LHC and $\sim 250\,\text{GeV}$ for Tevatron. Also, as expected, the transverse momentum was not distorted due to the Lorentz boost. The angular distributions in fig. 4.4 show now forward-backward asymmetry. However, at LHC the top quarks are preferably generated at an angle of $0°$ or $180°$, whereas at Tevatron the distribution is almost isotropic. However, this is not the property of a proton-proton collider but due to the higher collision energy.
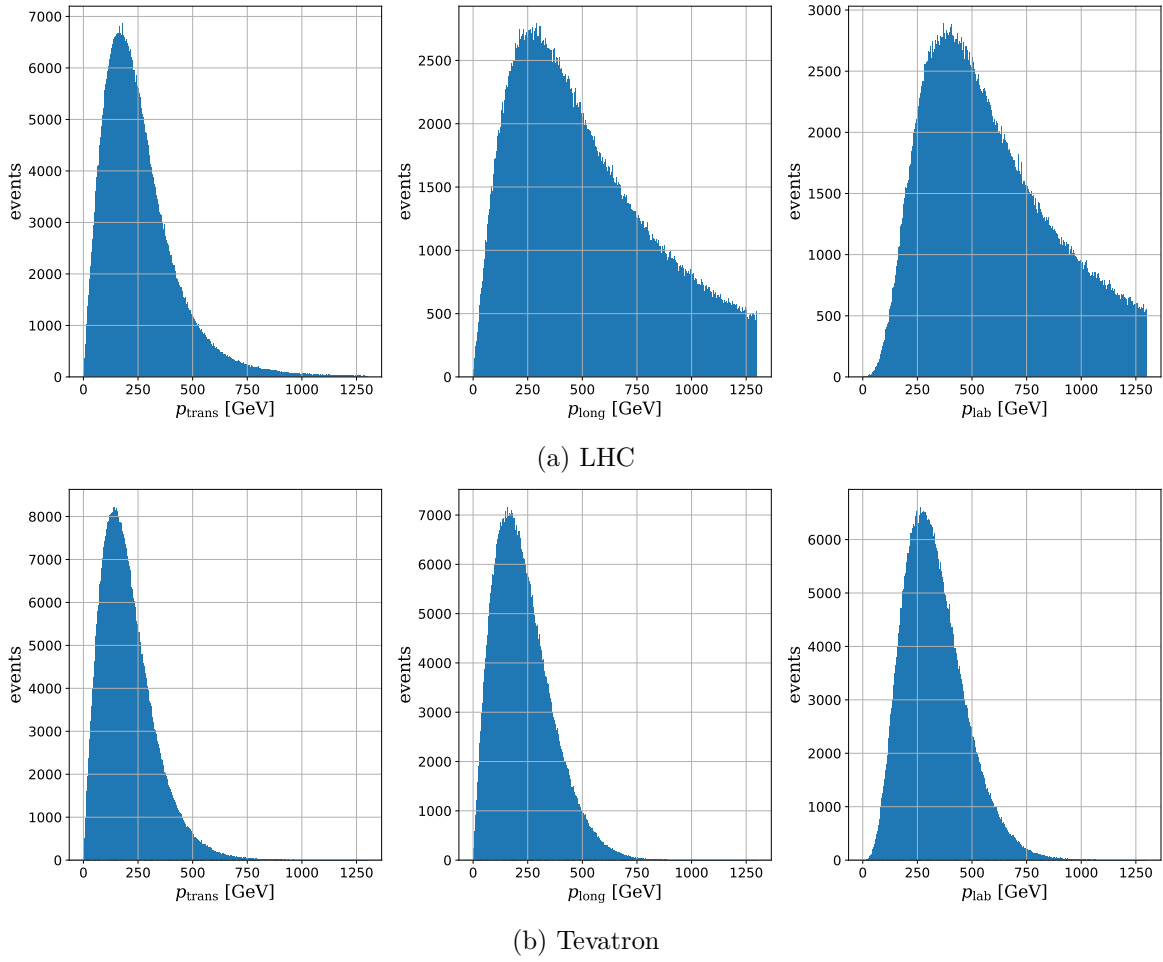
(a) LHC

(b) Tevatron

Figure 4.3: Transverse, longitudinal and total momentum of the generated events in the lab frame presented as histogram.
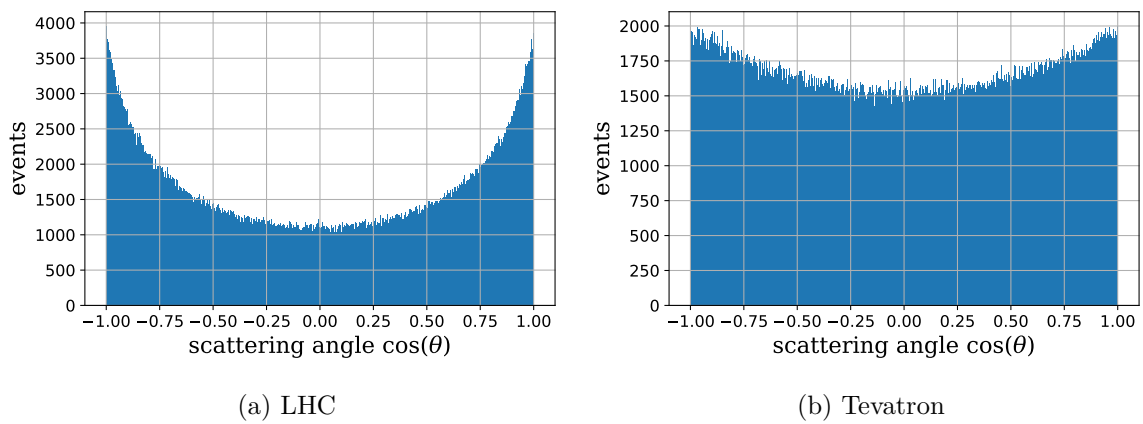

(a) LHC

(b) Tevatron

Figure 4.4: Angular distribution of the generated events presented as histogram. No forward-backward asymmetry can be detected.

5 Conclusion and outlook

The total hadronic cross section for top quark pair-production at tree level for pp and $p\bar{p}$ collider was calculated in this thesis and compared with the ones generated by the program TOP++ [4]. Both programs lead to the same results within the numerical uncertainties. However, the results depend heavily on the choices made for the renormalization and factorization scale. The inclusion of higher orders perturbation theory would reduce the scale dependence and improve the predictions. In addition, it was confirmed that at Tevatron $92\,\%$ of the top quarks are produced through quark-antiquark annihilation while gluon fusion is the dominant production channel at LHC with a share of $86\,\%$ [3, p. 2]. The event generation has shown that no forward-backward asymmetry is expected at both colliders, the LHC and the Tevatron, at least with a leading order event generator. Furthermore, most top-antitop pairs are not produced at an energy corresponding to the top quark mass but at a higher energy. However, the full predictive power of a Monte Carlo generator only becomes apparent when the results of the simulation are compared with actual measurement data. So, the next step is to compare the generated events with data obtained at the CMS or ATLAS detector.

Bibliography

[1]   Andy Buckley et al. "LHAPDF6: parton density access in the LHC precision era". In: *Eur. Phys. J.* C75 (2015), p. 132. DOI: `10.1140/epjc/s10052-015-3318-8`. arXiv: `1412.7420 [hep-ph]`.

[2]   Matteo Cacciari et al. "Updated predictions for the total production cross sections of top and of heavier quark pairs at the Tevatron and at the LHC". In: *JHEP* 09 (2008), p. 127. DOI: `10.1088/1126-6708/2008/09/127`. arXiv: `0804.2800 [hep-ph]`.

[3]   Giorgio Cortiana. "Top-quark mass measurements: Review and perspectives". In: *Reviews in Physics* 1 (2016), pp. 60–76. ISSN: 2405-4283. DOI: `https://doi.org/10.1016/j.revip.2016.04.001`. URL: `http://www.sciencedirect.com/science/article/pii/S2405428316300028`.

[4]   Michal Czakon and Alexander Mitov. "Top++: A Program for the Calculation of the Top-Pair Cross-Section at Hadron Colliders". In: *Comput. Phys. Commun.* 185 (2014), p. 2930. DOI: `10.1016/j.cpc.2014.06.021`. arXiv: `1112.5675 [hep-ph]`.

[5]   Sayipjamal Dulat et al. "New parton distribution functions from a global analysis of quantum chromodynamics". In: *Phys. Rev.* D93.3 (2016), p. 033006. DOI: `10.1103/PhysRevD.93.033006`. arXiv: `1506.07443 [hep-ph]`.

[6]   F. Halzen and Alan D. Martin. *QUARKS AND LEPTONS: AN INTRODUCTORY COURSE IN MODERN PARTICLE PHYSICS*. 1984. ISBN: 0471887412, 9780471887416.

[7]   Frederick E James. *Monte Carlo phase space*. eng. 1968. DOI: `10.5170/cern-1968-015`. URL: `http://cds.cern.ch/record/275743`.

[8]   Matthias Jamin and Markus E. Lautenbacher. "TRACER: Version 1.1: A Mathematica package for gamma algebra in arbitrary dimensions". In: *Comput. Phys. Commun.* 74 (1993), pp. 265–288. DOI: `10.1016/0010-4655(93)90097-V`.

[9]   P. Nason, S. Dawson, and R.K. Ellis. "The total cross section for the production of heavy quarks in hadronic collisions". In: *Nuclear Physics B* 303.4 (1988), pp. 607–633. ISSN: 0550-3213. DOI: `https://doi.org/10.1016/0550-3213(88)90422-1`. URL: `http://www.sciencedirect.com/science/article/pii/0550321388904221`.

[10]   Andreas Papaefstathiou. "How-to: Write a parton-level Monte Carlo event generator". In: (2014). arXiv: `1412.4677 [hep-ph]`.

[11]   Michael E. Peskin and Daniel V. Schroeder. *An Introduction to quantum field theory*. Reading, USA: Addison-Wesley, 1995. ISBN: 9780201503975, 0201503972. URL: `http://www.slac.stanford.edu/~mpeskin/QFT.html`.

[12]   Matthew D. Schwartz. *Quantum Field Theory and the Standard Model*. Cambridge University Press, 2014. ISBN: 1107034736, 9781107034730. URL: `http://www.cambridge.org/us/academic/subjects/physics/theoretical-physics-and-mathematical-physics/quantum-field-theory-and-standard-model`.

[13]   Peter Skands. *QCD for Collider Physics*. 2011. arXiv: `1104.2863`.